Recent Progress of Concrete/Steel/FRP Hybrid Structures

Proceeding

International Joint Seminar of the KSCE and the JSCE
2006 KSCE Annual Conference
Gwangju, Korea
October 13, 2006

Editors

Ha-Won Song
Hiroshi Yokota

Co-organizer

Structure Committee of Korean Society of Civil Engineers

Hybrid Structure Committee of Japan Society of Civil Engineers

PREFACE

An International Joint Seminar on theme of *'Recent Progress of Concrete/Steel/FRP Hybrid Structures'* is jointly organized by the Structure Committee of Korean Society of Civil Engineers (KSCE) and the Hybrid Structure Committee of Japan Society of Civil Engineers (JSCE). It is held during the Annual Conference of KSCE at Gwangju, Korea on October 13, 2006 as a product of an international cooperation between the KSCE and the JSCE.

The purpose of this joint seminar is to exchange information for the recent progress on the hybrid structures and to discuss the future developments. This proceeding consists of 6 valuable papers on the theme. I wish the ideas presented in the seminar will be useful and informative to those who attend the seminar and will be the valuable materials for the advancement of technology of the hybrid structures in both countries and world. I also hope the occasion shall deepen the friendship and explore cooperation among participants. On behalf of the Structure Committee of KSCE, I would like to take this opportunity to thank Prof. Ha-Won Song and Dr. Hiroshi Yokota for their devoted preparation for this seminar. Once again I would like to express my sincere gratitude to the all speakers and participants for their valuable contribution.

Sung Woo Lee, Ph.D.
Chair of Structure Committee
Korean Society of Civil Engineers

Content

JSCE-KSCE Joint Seminar on Progress of Hybrid Structures – Background from JSCE –

UEDA Tamon
Hokkaido University, Japan

Abstract
This brief report describes the background of holding the JSCE-KSCE Joint Seminar on Progress of Hybrid Structures, especially on the JSCE side. For this purpose a newly established JSCE Committee on Hybrid Structures is also briefly introduced.

1. Introduction

Hybrid structure is defined in Japan as a general term meaning both composite structure and mixed structure. Composite structure is a structure consisting of composite members in which different materials are used in its cross section, such as steel-concrete composite beam and steel reinforced concrete column. Mixed structure is a structure consisting of different types of members, such as reinforced concrete column and steel beam. Because of greater choices of material and member types, hybrid structures are likely to show advantages to its competitor, concrete and steel structures and getting more popular in Japan and the world.

Design methods for both concrete and steel structures have been well developed, which are different. Hybrid structures, in which typical materials used are concrete and steel at present, are between concrete and steel structures, meaning that existing design methods for concrete and steel structures cannot be applied directly. Besides variety of materials and members in hybrid structures is great and makes its design method more complicated.

Associations for both concrete and steel structures have been existing domestically and internationally among professional engineers and academics. However, associations for hybrid structures are not the case. Due to this fact there is scarcely exchange of information on hybrid structures, such as its design method.

This is the primary reason for Committee on Hybrid Structures in JSCE to propose a joint seminar between JSCE and KSCE. JSCE recognized its importance and granted financial support to the Joint Seminar, while KSCE included it as a part of International

Programs during 2006 KSCE Annual Conference.

2. JSCE Committee on Hybrid Structures

There are two committees, Concrete Committee and Committee on Steel Structures, in JSCE which take a care of concrete and steel structures respectively. A Joint Sub-committee on Steel-Concrete Composite Structures had been actively working under Concrete Committee, Committee on Steel Structures and Committee on Structural Engineering for more than a decade. Finally it became an independent committee, Committee on Hybrid Structures, in 2005.

Committee on Hybrid Structures expanded its scope by not limiting to steel-concrete composite structures and but dealing with the other materials, such as FRP and geo-materials, and mixed structures. One of the primary tasks is to maintain Guidelines for Performance-Based Design of Steel-Concrete Hybrid Structures, which was published for the first time in 2002. This is the first with the performance-based concept for hybrid structures, and its English-translated version was published in 2006.

Currently there are an Executive Committee and eight sub-committees in the Committee as follows:

- Sub-Committee on Performance-Based Guidelines
- Sub-Committee on State-of-the Art
- Sub-Committee on Maintenance
- Sub-Committee on Hybrid Technology with New Materials
- Sub-Committee on FRP Hybrid Bridges
- Sub-Committee on Repair and Strengthening of Steel and Hybrid Structures by FRP
- Sub-Committee on International Affairs
- Sub-Committee on Symposium on Application of Hybrid Structures

3. Concluding Remarks

Through the Joint Seminar, I, as Chairman of Committee on Hybrid Structures, strongly hope that more collaboration on hybrid structures between JSCE and KSCE could be made in the coming years and that the collaboration could bring out international leadership in hybrid structures, such as proposing an international code which has not existed for hybrid structures.

ADVANCED COMPOSITE MATERIALS IN BRIDGE DECKS AND HYBRID MARINE PILES

Sung Woo Lee (swlee@kookmin.ac.kr), Kee Jeung Hong (kjhong@kookmin.ac.kr)
Kookmin University, Seoul, Korea

Abstract

Due to many advantage such as high strength, high durability and light weight, advanced composite materials are considered one of the promising alternative to conventional construction materials. In this paper, some of the recent research developments on the glass fiber reinforced composite bridge deck and the hybrid composite marine pile are presented. For the pultruded composite bridge deck of hollow section profile, structural performance is studied through extensive analysis and experiments. It also presents some of the field application for the developed bridge deck. For the filament wound composite pile filled with concrete, experimental and analytical studies on the constitutive law and axial-flexural behavior are carried out, and some of the results are presented.

1. Introduction

To cope with problems of deterioration and corrosion of conventional steel and concrete materials, high durable, light-weight fiber reinforced composites are considered as one of promising alternative construction materials for the civil infrastructures. Among many applications, composite bridge decks and marine piles seem to be most notable.

Composite bridge deck has significant advantages compared with conventional concrete deck since it is high durable and corrosion-free. Much longer service life and lower maintenance cost are expected so that much lower life-cycle cost (LCC) of the bridge structure can be achieved. Due to lightweight characteristics, the composite bridge deck can reduce the dead load as much as 80% of that of conventional concrete deck. Because of the reduced dead load, much slender bridge substructures can be possible. When the composite bridge deck is used for re-decking, load carrying capacity of the bridge is upgraded automatically without strengthening girder or substructures. Furthermore, due to fast installation of the composite decks, it reduces construction duration and traffic block time significantly, so that considerable savings of direct and indirect costs can be achieved. Due to notable advantages of composite bridge deck as

mentioned above, many studies were carried out and increasing field applications were reported recently [1,2]. Many composite deck profiles has been developed and used in practice from 1990's [2]. United States are leading the R&D of composite bridge deck and there are already more than 200 bridges including pedestrian bridges in use. In Korea more than 10 composite deck bridges are in use and increasing number of composite deck bridges are designed recently. At the end of the year 2006, the total area of composite deck installed in Korea is expected to be 13,000m^2, which is more than 8,000m^2 in U.S.. In this paper, structural performance of glass fiber reinforced composite bridge deck (called 'Delta Deck') of 3-cell trapezoidal profile, which is fabricated with pultrusion, is investigated under the DB24 Korean highway truck load. Extensive experiments including flexural, and field load tests for the pultruded deck are conducted. Some field applications of developed composite deck are presented as well. It also describes the next generation of deck profile with vertical snap-fit connections.

Concrete filled glass fiber reinforced polymer (GFRP) pile has been introduced to overcome the corrosion and deterioration issues of steel and concrete piles under severe environments [3]. Benefits of composite piles include high durability, high confined strength, high ductility, low maintenance cost, and long expected service life. Because of these benefits, increasing applications of composite marine pile are reported in United States. It is considered the most viable alternative to timber pile which is not safe against marine borer's damage. Although the composite tube itself possesses high strength, its elastic modulus is significantly low compared with concrete material. Thus the inner part of the tube shall be filled with concrete to increase compressive loading capacity and also to increase resistance to lateral deflection. Investigation has been carried out to examine material and structural characteristics of GFRP piles. It includes the compressive test for short length composite tubes and axial-flexural test under various load combinations. Numerical procedure to construct P-M diagrams for composite piles is also developed and the results are compared with experiments. Present study will demonstrate the applicability of concrete filled glass fiber reinforced composite piles as an alternative to conventional steel or concrete piles in corrosive environments, and provide an experimental database on the multi-directionally reinforced composite piles.

2. Composite Bridge Deck

2.1 Design and Fabrication of Composite Deck

Pultrusion is considered to be most economical fabrication method for composite structural members and it assures uniform product quality. Based on the previous studies on the composite deck, a deck profile for pultrusion is developed [4]. To satisfy serviceability criteria of local deflection and to improve fatigue characteristics of local behavior of top flange, a trapezoidal-shape section of 200mm depth as shown in Figure 1 is designed for the DB24 Korean highway truck load (rear axle load of 94.1kN) for

typical girders of 2.5m spacing. The profile consists of 3 trapezoidal sections and it will be bonded together to make complete deck panel. Considering local effect due to tire contact at the top surface, top flange is designed 16mm~20mm thick, which is thicker than 12mm-thick bottom flange. The web is 8mm thick. Laminate design is different each other for top flange, bottom flange and web. For pultrusion process with 60 % weight fraction of glass fiber is selected in the design. In the laminate, 8800 Tex E-glass roving is used in the longitudinal direction and multi-axial stitched fabrics (90°/±45°) are used for transverse direction. Unsaturated polyester is used as resin base of the composite deck. Figure 2 shows pultrusion fabrication process for the designed composite deck.

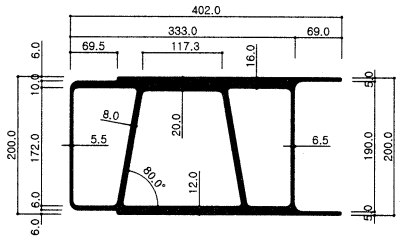

Figure 1. Profile of pultruded deck (Delta Deck)

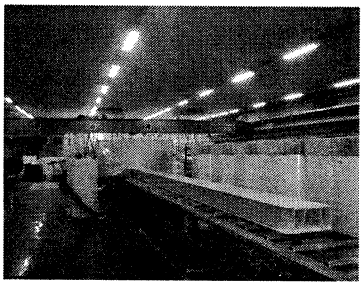

Figure 2. Pultrusion process of composite deck

2.2 Flexural Test for Pultruded Deck

Three-point flexural test is carried out in order to evaluate the structural performance of the pultruded composite deck. At failure load, flexural capacity and deflection of the deck are evaluated. Load is applied on the wheel load contact area of 580mm x 230mm. Test deck is 2.25m long, 1.0m wide and is simply supported. The load is applied at the center of the span.

Vertical deflections of the deck is measured through DT's positioned at 3 locations along the transverse line located at the middle of the span. Strains are measured at 16 points on the top and bottom flange of the deck. Figure 3 shows the locations of strain gages attached to the deck. Character 'L' indicates longitudinal direction and character 'T' indicates transverse direction of the deck in the figure.

Final failure mode of the flexural test turns out to be local punching failure of the top flange at the loading area (Figure 4). At failure, the load is 411.9kN and vertical deflection is 35.6mm. Since the rear axle load of DB24 including impact factor 1.3, is 122.4kN, factor of safety becomes 3.36 (411.9/122.4) for the simply supported condition. However, if the effect of load distribution beyond a 1.0m-width test deck and actual continuous support condition of the bridge are considered, it can be expected to have further safety margin.

The punching type failure mode shown in Figure 4 may not be anticipated to occur in real situation for the rubber tire contact, which is different from the experimental loading simulation. If real situation of tire loading is considered, it is anticipated to have more safety margins. FE analysis is also carried out for the test deck model. Although it is not included in this paper, the analytical results agree well with those from experiments [4]. In the analysis, Tsai-Wu failure index was also evaluated for the failure load of 411.9kN. Tsai-Wu failure indices for each strain gage location are shown in Table 1.

As shown in Table 1, maximum failure index at load location of top flange is 0.41. This means that the local failure occurs at 411.9kN load before the estimated global flexural failure occurs at 1000.3kN.

Though not included in this paper, many other tests, including shear test for girder-deck connection, compression fatigue test, flexural fatigue test, performance test for deck-barrier, shear and bonding test for pavement, vehicle generated noise test, accelerated weather test and chemical test for the coupon, are conducted and verified in various aspects of the composite bridge deck for use in the practice.

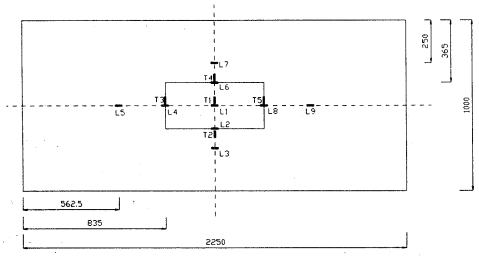

Figure 3. Location of the strain gages attached to top and bottom flanges

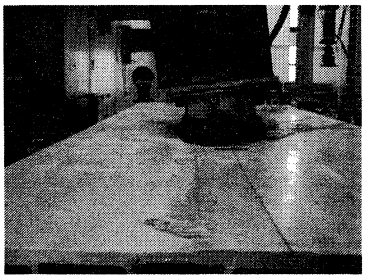

Figure 4. Failure mode at maximum load

Table 1. Tsai-Wu failure indices for strain gage location

	Gage No.	Tsai-Wu failure index		Gage No.	Tsai-Wu failure index
bottom flange	L1	0.23	top flange	L1	0.41
	L2	0.18		L2	0.26
	L3	0.04		L3	0.18
	L4	0.12		L4	0.28
	L5	0.02		L5	0.06
	L6	0.01		L6	0.36
	L7	0.04		L7	0.19
	L8	0.05		L8	0.18
	L9	0.02		L9	0.07

2.3 Field Applications, Analysis and Field Load Test

Construction of the Gwangyang Bridge

150m-long and 12m-wide plate girder bridge with pultruded composite deck was constructed at Gwangyang in October, 2004. Figure 5 and 6 show the profile and cross section of the bridge, respectively. Figure 7 shows installation of composite deck. Figure 8 shows heavily loaded traffic over the bridge after construction completed. For the constructed bridge, the finite element analysis and the static and dynamic field load tests are carried out as described below.

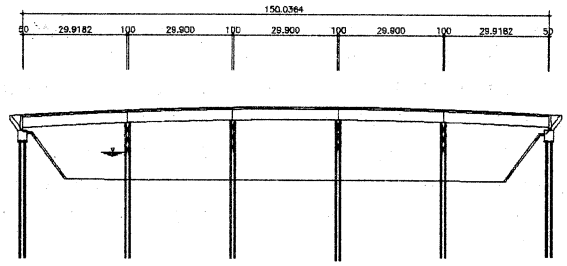

Figure 5. Profile of the Gwangyang Bridge

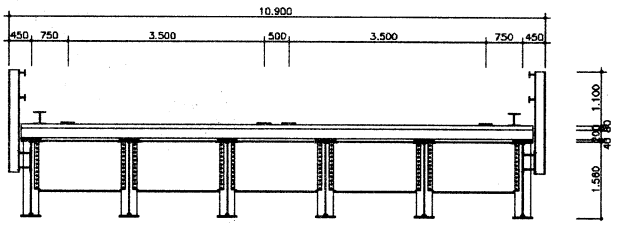

Figure 6. Cross section of the Gwangyang Bridge

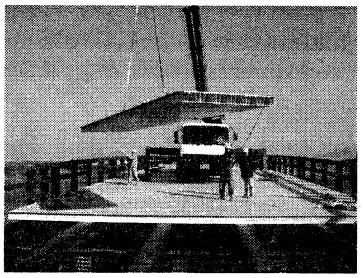

Figure 7. Installation of composite decks

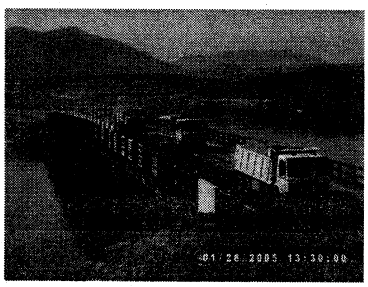

Figure 8. Heavily loaded traffic over the built bridge

Analysis

The bridge is 150m in length with simple supports and has 5 girders with 2.0m spacing. Finite element analysis is performed to examine serviceability and structural safety of the 'Delta-Deck' installed for the Gwangyang Bridge. The commercial FE analysis program 'COSMOS/M' is used in the analysis. The deck is modeled with shell elements with the material properties of the composites obtained by micromechanics. Rigid connecting elements are used for the connection between the deck and the girder. Figure 9 and 10 show the finite element models with test truck and DB24 truck loaded on the bridge respectively. The stress on the center of the deck at the location of gage T-1 in Figure 11 is calculated as 6.85 and 7.29MPa respectively for test truck and DB24 truck, which is very small values compared with ultimate strength 320 Mpa in the longitudinal direction of the deck tube. Due to low modulus of elasticity of the composite deck, normally if deflection serviceability criteria satisfy, it possesses large margin on the strength. The maximum static vertical displacements of the deck are calculated as 1.70 and 1.45mm respectively for the test truck and DB24 truck. Permissible deflection for the 2.0m girder spacing is estimated to be 4.71mm when deflection serviceability criterion of L/425 is applied. Thus it possesses 2.77 and 3.24 safety margin respectively for the permissible deflection.

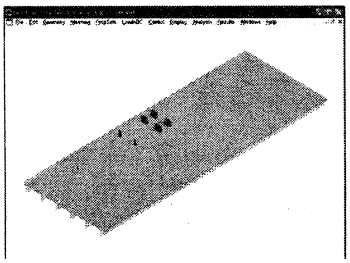

Figure 9. FE model for test truck

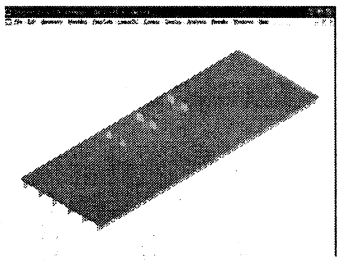

Figure 10. FE model for DB24 truck

Static Field Load Test

To measure the strains in longitudinal (L) and transverse (T) direction of the composite deck, the strain gages are installed at the locations as shown in Figure 11. To measure the vertical displacement, the displacement gages (DT) are also installed at the location as shown in Figure 11. The static load test is conducted with test truck loaded on the bridge at the same location as that used in the analysis (see Figure 9).

From the evaluation of the bridge, lowest factor of safety found at gage location L-4. The static stress at strain gage L-4 in Figure 11 is calculated as 2.10MPa from the measured strain for test truck. If it is converted to DB24 truck load using the analysis results, it becomes 5.61 Mpa. Therefore, considering dead load and DB24 live load with impact factor of 1.3, the factor of safety with respect to the ultimate strength of 96.2 Mpa in the deck transverse direction becomes 13.6.

Table 2 shows the measured vertical displacement from the static field load test at DT-1, DT-2 and DT-3 in Figure 11. The maximum relative deck displacement for the test truck is 1.50mm, which is 13% less than 1.70mm in the finite element analysis. Thus the serviceability safety margin of 3.13 is obtained for the test truck. When the test truck load is converted to the DB24 truck load, serviceability safety margin is estimated to be 3.67 for the static field load test and 3.24 for the finite element analysis. Both results from the static test and the analysis are found to satisfy the displacement criterion (L/425) of the Korean highway bridge code. Based on both the static field load test and the finite element analysis, the bridge is considered to possess sufficient strength and serviceability.

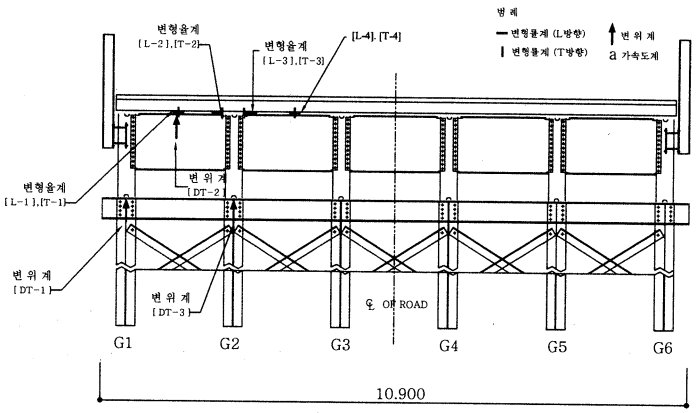

Figure 11 The location of instrumentation for the field load test

Table 2 Measured displacement from static field load test

Gage	Location	Displacement (mm)		Displacement criteria
		Load test	FE Analysis	
DT1	Center of girder G1	5.1	12.4	4.71mm (2000/425)
DT2	Center b/w G1 & G2	4.3	13.0	
DT3	Center of girder G2	2.8	11.3	
Relative deck displacement for the test truck, (DT2-DT3). [F.S.]		**1.50** [3.13]	**1.70** [2.77]	
Converted deck displacement for DB24 truck. [F.S.]		1.28 [3.67]	1.45 [3.24]	

Dynamic Field Load Test

In order to investigate the dynamic characteristics of the Gwangyang Bridge, dynamic field load tests are also conducted. The same test truck used in the static test is used

with four different vehicle velocities; 5km/h, 20km/h, 40km/h and 50km/h. The same gages shown in Figure 11 are used to measure strains and vertical displacements.

Figure 12 shows dynamic strain response of the deck measured at gages L-1 and L-2 when the truck runs with 50km/h velocity. Figure 13 shows the displacements of the deck (DT-2) and girders (DT-1 and DT-3) when the truck runs with 50km/h velocity. The maximum flexural stress is 3.04MPa converted from the measured strain for the quasi-static crawl velocity (5km/h). The maximum stress at negative moment location is 2.35MPa converted from the measured strain near girder G2 for the velocity of 40km/h. Since these stresses are comparatively very small, the bridge is justified to be safe also for the dynamic loads.

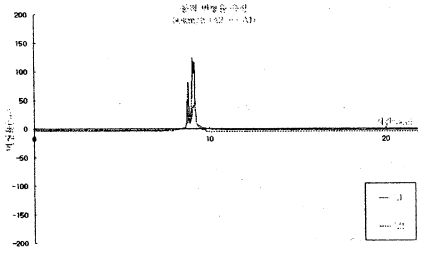

Figure 12. Dynamic strain response (50km/h velocity)

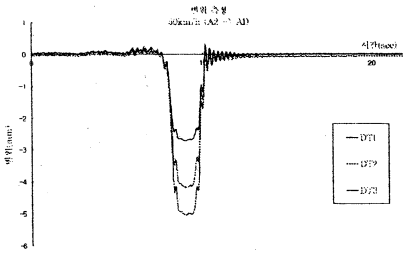

Figure 13. Dynamic vertical displacement response of the deck (50km/h velocity)

Table 3 Measured displacement of the deck from dynamic field load test

Loading case	Deck displacement = DT2 - DT3 (mm), [F.S.]					Displacement criteria
	5km/h	20km/h	40km/h	45km/h	50km/h	
150kN test truck	1.49 [3.15]	1.47 [3.20]	1.46 [3.22]	1.46 [3.22]	1.47 [3.20]	4.71mm (2000/425)
Converted for DB24 design truck	1.27 [3.70]	1.25 [3.76]	1.24 [3.79]	1.24 [3.79]	1.25 [3.76]	

Table 3 shows the measured vertical displacements of the deck for different velocities of the truck. The maximum vertical displacement is 1.49mm at the mid-span of the deck, which is much less than 4.71mm (L/425), the permissible displacement criteria of the Korean highway bridge code. These displacements are measured when the 150kN test truck moves on the bridge, and they are converted for the DB24 design truck loading. The converted displacement is 1.27mm, which is even smaller than that of the test truck

load. Therefore, the bridge is considered to be stiff enough to provide sufficient serviceability.

The World Largest Composite Deck Bridge

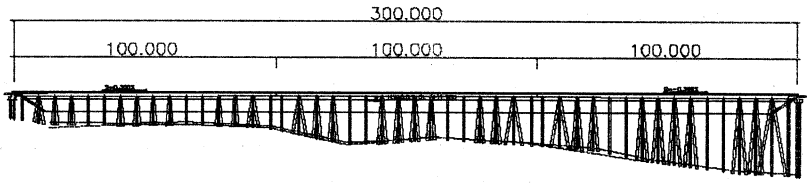

Figure 14. Profile of Noolcha Bridge at Busan port

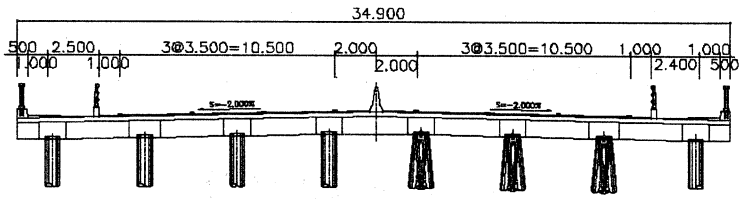

Figure 15. Cross section of Noolcha Bridge

Figure 16. Pile foundation of Noolcha Bridge before installation of decks

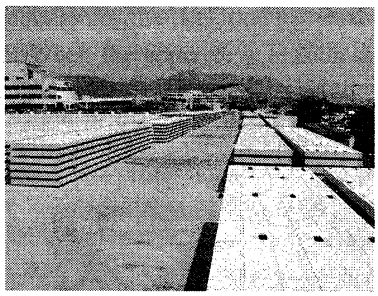

Figure 17. Yard storage of composite deck panels before installation

A wharf-type girder bridge, Noolcha Bridge, which is 300m-long and 35m-wide, in Busan new port area is currently under construction and expected to be completed in early 2007. This bridge will be the largest composite deck bridge in the world when it is completed. Composite deck was selected for this bridge due to the benefits from construction cost savings and efficient maintenance. Light-weight property of the deck significantly reduces the number of foundation marine piles so that initial construction cost was lowered considerably. In addition, due to highly durable property of the deck,

life-cycle cost can also be lowered remarkably. Figures 14 and 15 show the profile and cross section of Noolcha Bridge, respectively. Figure 16 shows the marine pile foundation of Noolcha Bridge before installation of composite decks. These decks are stored on the yard and prepared for installation as shown in Figure 17.

2.4 Snap-Fit Connection for Next Generation of Composite Deck

Until now, tongue and groove method is the only way for the composite deck connection. For the composite bridge decks of tongue and groove type, to assemble the deck panels one another on top of the girder, they should be pushed in horizontal direction with adhesive bonding. Then shear connectors are installed to the girder from the top of the panel through the pre-drilled hole after the deck panels have been assembled. However, the workability and construction quality can be bad in this case.

In the conventional bridge deck construction practice, the shear connectors are installed on top of the girder prior to deck placement. To improve this situation, it is necessary to develop the method of deck panel assembly in the vertical direction. Vertical snap-fit connection method is considered one of the solutions to the problems of this kind.

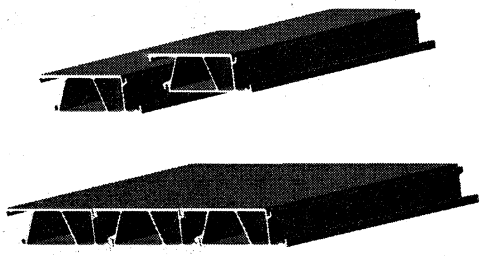

Figure 18. Concept of vertical snap-fit connection for the composite bridge decks

The concept of vertical snap-fit connection for the composite bridge deck is shown in Figure 18. This method has been in use for plastic products such as toys, camera, electronic circuit board, etc, but has not been used so far for large structures [5].

Various profiles of the snap-fit connections are studied currently. Figure 19 shows analysis result simulating snap-in and snap-out for one of the models of snap-fit connection. The connections are modeled with solid elements using material properties calculated by the layer analysis done by ESAComp. Also, geometric nonlinearity is considered to accurately simulate the behavior of the flexible arms in the connections. Figure 20 shows the pedestrian bridge constructed with the developed composite decks having snap-fit connections at Wolchul mountain in Korea.

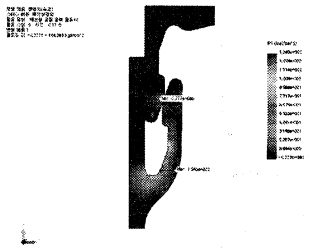

Figure 19. Analysis for snap-in and snap-out

Figure 20. Installation of snap-fit composite deck for a pedestrian bridge

3. Hybrid Composite Marine Pile

3.1 Constitutive law for Concrete-Filled Composite pile

The structural characteristics of concrete filled hybrid composite pile are studied in this paper. Various composite tubes with different thickness and fiber directions are fabricated with filament winding and filled with concrete. The filled-in concrete in the tube have design strength of 40MPa at 28 days. Many uni-axial compression tests are conducted and Figure 21 shows one of the such tests.

Figure 23 shows results for the experimental stress-strain curves in the axial direction for the concrete filled composite tube. Labels 1~4 in the figure simply represent specimen ID. It is recognized that the stress-strain curve can be divided into two parts; first part showing high stiffness, and second part revealing high ductility due to confinement effect. The strengths of the concrete-filled FRP tubes are 2.0 ~ 2.4 times higher than those of plain concrete cylinders. Revealing high ductility, the strains at failure are also 5.3 ~ 7.0 times higher for FRP tubes. Figure 22 shows theoretical constitutive model for the FRP-encased concrete by Samann [6] based on similar experiments described above.

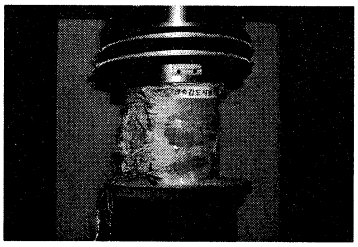

Figure 21. Uni-axial compression test for concrete-filled composite tubes

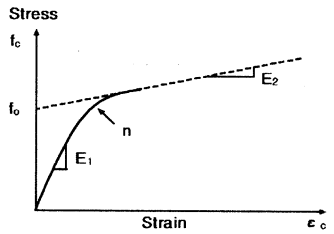

Figure 22. Constitutive model for FRP-encased concrete [6]

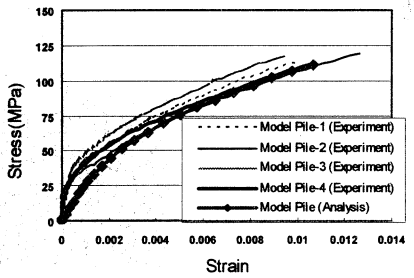

Figure 23. Stress-strain relations of concrete filled composite tubes (experiments and analysis)

The bilinear constitutive law of GFRP confined concrete in Figure 22 is represented by a relation given by the following equation [6].

$$f_c = \frac{(E_1 - E_2)\,\varepsilon_c}{\left[1+\left(\frac{(E_1 - E_2)\,\varepsilon_c}{f_o}\right)^n\right]^{1/n}} + E_2\,\varepsilon_c \tag{1}$$

In Eq. (1), n=1.5 and other notations in this equation are given in Figure 22. By conducting some separate tube tests, the first and second slopes of the stress-strain curve in Figure 22 are obtained. By varying fiber volume, a series of stress-strain relations are obtained. Using results of tensile tests of composite tubes and compression tests of concrete-filled composite cylinders of various fiber volumes, the constitutive model of hybrid composite pile can be represented. Based on theses experimental results, the relation between the elastic modulus ratio (E_2 / E_1) and the stiffness ratio ($E_h t / f_{co} D$) is determined as shown Eq. (2) by fitting the experimental data [3].

$$E_2 = E_1\left[0.0009 \cdot \frac{E_h t}{f_{co} D}\right] + 0.281 \tag{2}$$

where E_h is modulus of elasticity in the hoop direction, t is tube thickness, f_{co} is compressive strength of unconfined concrete, and D is inner diameter of the tube. Figure 23 shows that the analytical prediction calculated by Eqs. (1) and (2) agrees well with the experimental results.

3.2 Axial-Flexural Tests

Seven concrete filled composite piles are tested under axial-flexural load (P-1 through P-7; diameter=165mm, length=1200mm). The properties of these piles are shown in Table 4. After predetermined axial load is applied, flexural force is applied next. The flexural force is applied by four-point bending setup as shown in Figure 24. Figure 25

shows failure mode for one of the composite piles tested. Initial axial forces, failure axial forces and failure moments are given in Table 5.

Table 4. Properties of composite piles tested

Property		Value	Property	Value
Layer		L900-5PLY FW-2PLY	Total tube thickness (mm)	6.7
Fiber volume for HL (%)		35	Inner diameter (mm)	165.2
Fiber volume for FW (%)		50	Filled concrete strength (MPa)	40
Ply thickness (mm)	0°	4.85		
	90°	1.82		

Table 5. Initial axial force, failure axial force and failure moment of each tested composite piles

Member ID	Initial axial force (kN)	Axial force at failure (kN)	Moment at failure (kN·cm)
P-1	196.14	235.17	9188.55
P-2	294.21	337.26	9264.60
P-3	588.42	400.62	9330.65
P-4	784.56	426.90	9256.60
P-5	980.70	578.02	9867.04
P-6	1176.84	1174.98	6702.78
P-7	1372.98	1335.22	6864.90

Tension failure is occurred for member P-1~P-5. When the concrete in tension starts to crack as the load increases and the outside tube takes over the moments. Therefore final flexural strength is determined by the yield strength of the glass fibers at the tension side.

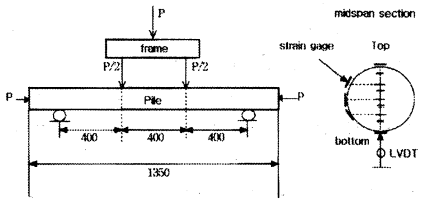

Figure 24. Axial-flexural test setup

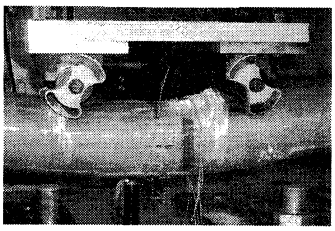

Figure 25. Failure mode of axial-flexural test

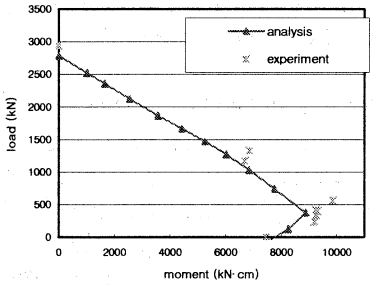

Figure 26. P-M interaction diagram by analysis and experiments

Compression failure is examined at the top surface of test member P-6~P-7 because of the larger axial force. It is found that the slopes of the load-displacement curves decrease as the load increases for all test cases. It is confirmed that concrete-filled GFRP tubes show ductile failure for both uni-axial compression and axial-flexural load cases.

A P-M interaction diagram is developed using a theoretical computation based on the tensile strength of fibers and compressive response of confined concrete [3]. Figure 26 shows axial-flexural test results along with computed P-M interaction diagram. As shown in the figure, they agree well each other. Thus it is considered that the developed P-M interaction diagram provides good prediction of the concrete filled composite piles of the kind studied in this paper.

4. Concluding Remarks

In this paper, some of the recent research developments on the glass-fiber-reinforced composite bridge deck and the hybrid composite marine pile are presented.

Studies for design, fabrication and experiment, and some field applications of fiber-reinforced composite bridge decks are presented. Deck profile for pultrusion is designed and fabricated for the DB24 Korean highway truck load. Extensive analyses and experiments are carried out for this pultruded deck. It is demonstrated that developed pultruded composite deck possesses enough safety factors for strength and serviceability well beyond the requirements of Korean highway code. Some field applications for composite deck bridge in Korea are also described. The new generation of composite deck having vertical snap-fit connection is introduced. Due to many advantages of composite bridge deck such as light-weight, high durability, high strength and fast installation, it is anticipated to be utilized widely in the civil infrastructures in the near future.

In addition to the study on the bridge decks, study on the structural characteristics of concrete-filled GFRP composite piles are also presented. This research verified the potentials of concrete-filled composite piles as an alternative to conventional compression members in corrosive environments. And it provides an experimental database for FRP composite piles that are externally reinforced by multidirectional fiber composites. Through this study, the following conclusions are drawn: 1) the axial strength of the concrete-filled GFRP tubes increases by a large amount due to the confinement effect given to concrete by the FRP shell, 2) significantly ductile failure is observed for both pure axial compression and axial-flexure load, 3) P-M interaction diagram is constructed based on the confined model of encased concrete, and sufficiently precise prediction is obtained, and 4) the role of bond between encased concrete and shell is essential to guarantee perfect integrity and increased the flexure performance of piles.

5. Acknowledgement

The study on the composite bridge decks presented in this paper are partly supported by Ministry of Construction and Transportation (Mokjeok A01) and Korea Science and Engineering Foundation(Grant no: R01-2004-000-10696-0). The other study on the composite marine pipe is sponsored by the Ministry of Maritime Affairs and Fisheries of Korea. The authors gratefully acknowledge its supports.

6. References

1. DARPA (2000), "Advanced Composites for Bridge Infrastructure Renewal-Phase II Tasks 16- Modular Composite Bridge", Defense Advanced Research Projects Agency, Technical Report Vol. IV, USA
2. Keller, Thomas (2003), "Use of Fiber Reinforced Polymers in Bridge Construction", *Structural Engineering Documents 7*, IABSE (International Association for Bridge and Structural Engineering), Switzerland
3. Lee, S.W. et al. (2002), "Development of Composite Marine Piles of High Durability," *Research Report KMU/SSRC-02/01*, Structural Safety Research Center, Kookmin University, Seoul, Korea
4. Lee, S.W. (2004), "Development of High Durable, Light Weight and Fast Installable Composite Bridge Deck", *MOCT R&D Report*, Ministry of Construction and Transportation, Korea
5. Lee, David E. and Hahn, H. Thomas (1996), Assembly Modeling and Analysis of Integral Fit Joints for Composite Transportation Structures, ASME Design Engineering Technical Conferences and Computers in Engineering Conference, August 18-22, Irvine, California.
6. Samaan, M., Mirmiran, A., and Shahawy, M. (1998), "Model of concrete confined by fiber composites." *J. Struct. Engrg.*, ASCE, 124(9), 1025-1031.

JSCE Guidelines for Performance Verification of Steel-Concrete Hybrid Structures

Hiroshi Yokota
Port and Airport Research Institute, Japan

Abstract
The Japan Society of Civil Engineers published the Guidelines for Performance Verification of Steel-Concrete Hybrid Structures in 2006. The Guidelines consists of six parts covering general principles, typical hybrid structural components such as composite beams, composite slabs and composite columns, and mixed structures. The Guidelines is the first officially published design guideline for hybrid structures based on the performance-based concepts in Japan. The three sets of structural performance are directly verified there; that is, safety, serviceability, and restorability. Durability is one of the important aspects to be considered in the design, but is not included there, because durability should be considered by the process of verification to each performance requirement achieved during the design life of structure. Therefore, durability is implicitly considered as changes in performance of structures with time. This paper introduces the outline of the Guidelines and principles for the performance verification of hybrid structures.

1. Introduction

The Japan Society of Civil Engineers (JSCE) is one of the professional bodies to prepare models for practical codes and standards for civil engineering structures through introducing the latest technological and research developments. As a part of these activities, the JSCE has already published two design codes/specifications for composite structures from the viewpoints of steel and concrete, respectively. The JSCE Joint-Committee on Steel-Concrete Composite Structures, the predecessor of the present Committee on Hybrid Structures, merged these two existing design codes as well as added knowledge after publication of them and newly issued the Guidelines for Performance Verification of Steel-Concrete Hybrid Structures in October 2002. Then, its English translated edition[1)] was published in March 2006. The Guidelines adopts the performance-based concept that is a new design concept being introduced in all kinds of design codes, specifications, etc. all over the world. The concept was clearly introduced in ISO standards, for example, ISO 19338-2003[2)].

The performance to be required and verified for designing hybrid structures include several aspects such as safety, serviceability, restorability, easiness of maintenance, demolition and recycle, constructability, and environment friendliness. Among them, safety, serviceability, and restorability are taken as primary performance that has to be directly verified. Safety is the ability of a structure or structural element to assure no casualty of users and people around the structure within the limits of acceptable probability. Serviceability is the ability of a structure or structural element to provide appropriate behavior or functionality in service under the possible actions at serviceability limit state. Restorability is defined as the ability of a structure or structural element to repair to the acceptable level of performance easily and economically, if damage occurs under the effects of considered actions. Durability is a very important aspect because it leads to the loss in structural performance due to deterioration of materials. In the Guidelines, therefore, durability is not directly verified but is to be achieved by verifying the performance in consideration of its change with time during the design working life of structure. Unfortunately no methods for verification of some of other performance are available at that moment. Requirement for economy should always be considered although it is out of the scope of any engineering documents, such as codes and standards.

The Guidelines covers hybrid structures of which fundamental structural materials are steel and concrete. The hybrid structures can be classified into the two categories: composite structures and mixed structures. A composite structure has a cross section with well-composed different kinds of materials, while a mixed structure consists of different types of steel, concrete, or composite members. In both structural categories, the Guidelines requires the smooth transmission of axial, flexural, and/or shear forces at the interface of different materials and at the joint between members. Therefore, not only conventional steel-concrete composite beams, concrete filled steel columns, steel encased concrete columns, and steel-concrete composite slabs, but also steel reinforced concrete (SRC) members (beams, columns, and slabs) and other new types of composite members are covered in the Guidelines.

The main table of contents of the Guidelines are as follows:

Part 1: General principle (common matters)
Part 2: Composite beam
Part 3: Composite slab
Part 4: Steel reinforced concrete column
Part 5: Concrete-filled tubular steel column
Part 6: Mixed structure
Appendix

The general principle in Part 1 refers to the common aspects that are applicable to all types of hybrid structures (composite and mixed structures), composite members (composite beams, slabs, and columns), and shear connectors. The following four parts

provide specific aspects for beams, slabs, and columns (columns are divided into two parts according to the methods of composition, such as verification methods for performance requirements, structural details, and construction. The part of mixed structure is prepared mainly for connection between different types of members. Several new types of hybrid structures are introduced in Appendices. Appendices also provide supplementary information on the main parts of the Guidelines.

2. General Principle

Part 1 "General Principle" consists of the following 8 chapters:

1. General rules
2. Performance requirement and method of verification
3. Action
4. Design values of materials
5. Structural analysis and calculation of response
6. Shear connectors
7. Structural details
8. Construction

In Chapter 1, scope of the Guidelines and definitions of terms and notations are described. Chapter 2 explains the concept of performance-based design, definition of each performance requirement, and general methods of verification. There are several ways to make verification properly including numerical analysis and experimental simulation. The limit state design methodology with the partial safety factor format is used to verity the required performance. For taking this approach, structural performance should be quantified in terms of performance indexes. Primary performance indexes are summarized in Table 1.

The level of performance requirements is given by specifying the *limit state* according to the limit state design methodology. The fundamental equation to verify the performance of structure is expressed as follows:

$$\gamma_i \frac{S_d}{R_d} \leq 1.0 \tag{1}$$

where,

γ_i: Structure factor
S_d: Design response (= $\gamma_a S(F_d)$)
S: Response of structure or structural member
γ_a: Structural analysis factor
F_d: Magnitude of action (design action or design load; = $\gamma_f F_k$)
F_k: Characteristic value of load and action
γ_f: Load factor

Table 1: Performance requirements and verification items and indexes

Performance requirement	Item of target performance	Verification item (limit state)	Example of verification index
Safety	Structure or member failure or collapse	Member failure	Stress resultant
		Fatigue failure	Stress resultant or stress
		Collapse of structure	Displacement and deformation of structure
		Instability of solid body	Displacement and deformation of structure or base
Serviceability	Comfortable use	Comfortable ride and comfortable walk	Acceleration and vibration frequency Displacement and deformation
		Appearance	Crack width Corrosion of steel
		Noise and vibration	Noise and vibration
	Impact to the third party	Local damage Appearance	Crack width and crack density
	Cover and penetration	Water tightness	Coefficient of permeability of structure Crack width
		Air permeability	Air permeability of structure Crack width
		Cover	Amount of leakage of material
		Penetration	Coefficient of permeability of structure Crack width
Restorability	Recovery of performance	Difficulty of restoration	Damage situation of member or structure

R: Critical value corresponding to verification item
R_d: Design resistance (= $R(f_d)/\gamma_b$)
f_d: Design strength of material (=f_k/γ_m)
f_k: Characteristic strength of material
γ_b: Member factor
γ_m: Material factor

In principle, changes in material properties with time due to environmental actions should be considered when calculating the response, S and the critical value, R in Equation 1. However, if appropriate measures against materials deterioration such as coating and corrosion protection are taken, changes in S and R with time may be negligible. Typical change in material property in hybrid structures is caused by corrosion of steel. Preventive measures against corrosion of exposed to air is generally coating or painting, while controlling the crack width and examining the carbonation

depth and the chloride ion penetration in concrete are probable kinds of measures for steel embedded in concrete.

Examination for corrosion of steel embedded in concrete due to carbonation of concrete can be carried out by Equation 2.

$$\gamma_i \frac{y_d}{y_{lim}} \leq 1.0 \tag{2}$$

where,

y_d: Design carbonation depth ($=\gamma_{cb} \alpha_d \sqrt{t}$)

γ_{cb}: Safety factor considering the variation of y_d
(=1.15 for normal concrete and 1.1 for high flowable concrete)

α_d: Design coefficient of carbonation

t: Elapsed time in years under carbonation (shorter than 100 years)

y_{lim}: Carbonation depth limit initiating corrosion over the steel

When the thickness of concrete cover to steel is 30 mm or more and the water-to-cement ratio of concrete is smaller than 0.5, deterioration due to carbonation may not be taken into account under normal environments.

For chloride-induced corrosion of steel, the following equation is applicable to verification:

$$\gamma_i \frac{C_d}{C_{lim}} \leq 1.0 \tag{3}$$

where,

C_d: Chloride content at the position of steel

C_{lim}: Threshold level of chloride to initiate corrosion of steel (generally, 1.2 kg/m^3)

For the calculation of chloride ion concentration, Fick's second law of diffusion is often applied to get the design diffusion coefficient of chloride ion in concrete, D_d. In case of cracks form in the cover concrete, D_d should be modified as a function of the width and spacing of cracks as follows:

$$D_d = \gamma_c D_k + \frac{w}{l}\left(\frac{w}{w_a}\right)^2 D_o \tag{4}$$

where,

D_d: Design diffusion coefficient of chloride ion in concrete

D_k: Characteristic value of diffusion coefficient of chloride ion in concrete

w: Crack width

l: Crack spacing

Table 2: Classification of interface between steel and concrete

	Rank A (elastic range) $S < S_y$	Rank B (yield acceptable) $S_y \leq S < S_u$	Rank C (full strength)
Level I (no separation)	I-A	I-B	I-C
Level II (elastic separation)	II-A	II-B	II-C
Level III (elasto-plastic separation)	-	III-B	III-C

S: Acting stress resultant in shear connector, S_y: Yield load-carrying capacity of shear connector, S_u: Ultimate load-carrying capacity of shear connector

w_a: Limit crack width relating to corrosion
D_o: Diffusion coefficient of chloride ion in cracked concrete (= 200 cm^2/year)

Limit values of crack width are set at $0.0035c$ to $0.005c$ (c: thickness of cover concrete) depending on environmental conditions. When Equations 2 and 3 are satisfied, steel corrosion would not occur during the design life due to carbonation and/or chloride ion. It means that the decrease in performance of hybrid structure does not occur under environmental actions.

As for actions, loads and environmental actions are considered in Chapter 3. The effects of environmental actions on structures and structural materials are considered for verification. Characteristic values for intensity of actions are provided separately for different limit states as confidence limits.

Chapter 4 shows how to obtain the design values of concrete and steel. Structural steel confined by surrounding concrete, which is often found in composite members, shows different strength from that without any confinement. Its characteristic value for strength in compression is assumed to be the same as in tension if it is fully confined and never buckled. Structural steel attached on concrete surface, which is not fully confined, indicates higher buckling strength than that without any confinement.

Shear connectors are very important structural components to achieve excellent mechanical behaviors of hybrid structures. In Chapter 6, shear capacity of various kinds of shear connectors, such as studs, steel shapes, and steel plates with openings (perforated-bond plate), are described with providing formulae for ultimate, fatigue, and serviceability limit states. An idea for the performance of shear connectors here is summarized in Table 2.

The level and category in the table relate to interfacial behavior in the serviceability limit

state and failure in the ultimate limit state respectively, which are defined as follows:

(a) Performance level for serviceability:

Level I: Neither the shear nor the separation of the material at the interface is allowed (moment resisting capacity is considered).

Level II: The shear connector and surrounding concrete are assumed in elastic region though the shear and the separation at the interface of connection are allowed (elastic connection).

Level III: Neither rupture of the shear connector nor slipping out of the concrete is admitted but the shear and the separation of the material at the interface are allowed. Also, partial yielding of the shear connector is allowed in this level (elasto-plastic connection)

(b) Performance level for safety

Rank A: All shear connectors are in the elastic region in the ultimate limit state of the structure (elastic range specification).

Rank B: The load-carrying capacity is not exceeded though a partial yielding of shear connectors is allowed in the ultimate limit state of the structure (yield acceptable specification).

Rank C: Neither rupture of the shear connector nor slipping out of the concrete is admitted though the deformation of the shear connector is large, and the plane remains plane assumption is disarranged in the ultimate limit state of the structure (full strength specification).

The performance of shear connector should be examined with the combination of above-mentioned levels and ranks to meet the performance requirement of composite beams, slabs and columns, and mixed structures.

For stud-type shear connectors, a formula for calculating the capacity under combination of shear force and pullout force is presented in Equation 5.

$$V_{sud} = \min\left[\left(\left(31A_{ss}\sqrt{(h_{ss}/d_{ss})f'_{cd}} + 10000\right)\Big/\gamma_b\right), A_{ss}f_{sud}/\gamma_b\right] \quad (5)$$

where,

A_{ss}: Cross-sectional area of a stud (mm^2)

h_{ss}: Height of a stud (mm)

d_{ss}: Shank diameter of a stud (mm)

$h_{ss}/d_{ss} > 4$

f'_{cd}: Design compressive strength of concrete (N/mm^2)

f_{sud}: Design tensile strength of a stud (N/mm^2)

γ_b: Member factor (= 1.3)

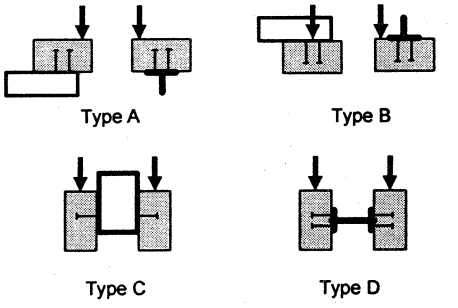

Figure 1: Definition of type of studs

Design capacity of studs depends on the direction of casting concrete as shown in Figure 1. For example, shear slip capacities of studs are 50% of V_{sud} for Types A and D stud, 30 % of V_{sud} for Type C stud, and 43 % of V_{sud} for Type B stud.

The chapter of construction (Chapter 8) describes appropriate processes for construction of steel and concrete components. The former includes treatment of interface between steel and concrete on the steel side.

3. Composite Beam

The part of composite beams describes individual matters applicable to them based on the basic principles (Part 1). The Part has the following 11 chapters:

1. General rules
2. Performance requirement and method of verification
3. Action
4. Design values of materials
5. Structural analysis and calculation of response
6. Verification of safety
7. Verification of serviceability
8. Verification of restorability
9. Verification of change in performance with time
10. Structural details
11. Construction

In Chapter 1, scope, definitions of terms, and notations are explained. Structural types dealt with in the Part are as follows:

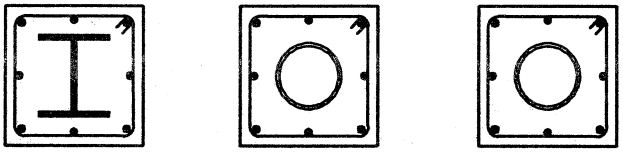

Figure 2: Typical cross sections of SRC beams

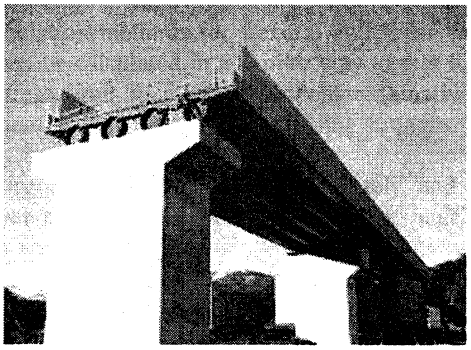

Figure 3: A railway bridge with new type composite beams
(Courtesy of Japan Railway Construction Public Corporation)

- Steel concrete composite beam consisted of steel beam and concrete slab: the compression part consists of concrete and the tension part of steel section. Steel and concrete are monolithically connected with shear connectors accordingly.
- Steel concrete composite beam with steel section embedded in concrete: steel sections are embedded into concrete such as steel reinforced concrete (SRC) as shown in Figure 2.
- Other new types of composite beam

An example of new type composite beam is shown in Figure 3. In this structure, concrete filled steel pipes are used as main girders of the railway bridge. The diameter of steel pipe is 1300 mm and spans of the bridge are 34 m+36 m+34 m.

For the verification of safety for conventional composite beams in flexure and axial force, classification of compact and non-compact sections is introduced. Design flexural capacity of SRC beam is calculated as a summation of design flexural capacities of reinforced concrete (RC) section under design axial force and steel section under design axial force. It is a prerequisite for verification that shear connectors between steel and concrete should not fail under the design loads. To assure this, the shear capacity for the ultimate limit state given in Part 1 has to be greater than the maximum shear force acting on the shear connector.

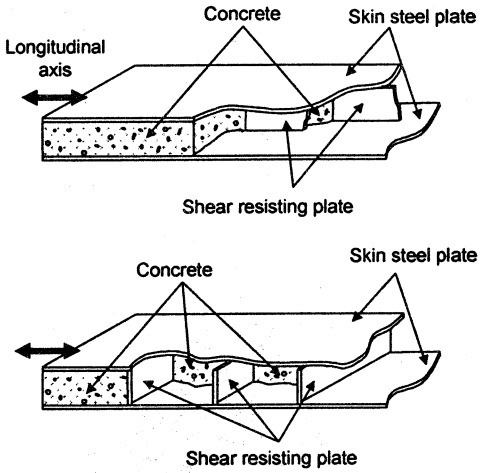

Figure 4: Steel-concrete sandwich slabs

Deformation is chosen as the performance index for verifying comfortable ride and walk. The verification can be conducted by the following equation:

$$\gamma_i \frac{\delta}{\delta_u} \leq 1.0 \tag{6}$$

where,

δ: Displacement or deformation of composite beam

δ_u: Critical value of displacement or deformation

γ_i: Structure factor

Deformation of conventional steel-concrete composite beams can be calculated by assuming its elastic behavior, while that of SRC can be obtained by the same way as that of RC members where average stiffness between cracked and un-cracked sections is used with consideration of time-dependent concrete deformation.

The width of crack on the surface of concrete is a performance index for verification of appearance and water-tightness. Crack width of concrete can be calculated by the same way as that of RC members.

4. Composite Slab

In this Part, the following composite slabs are referred to:

- Composite slab with embedded steel section: composite slab consisting of steel

sections or steel plate connected to steel skin plate as a formwork and filled concrete.

- Composite slab with steel plate: Composite slabs consisting of steel plate acting as a formwork as well as a structural component, shear connectors, and filled concrete
- Steel-concrete sandwich slab: composite slab in which core concrete is sandwiched by skin plates at top and bottom surfaces of the slab as shown in Figure 4.

The contents of the Part are the same as those of the part of composite beams. For safety verification, calculation methods for flexural and shear capacities are provided. The flexural capacity can be calculated in a similar way to that for RC members except for the compressive stress limit in steel component externally attached to concrete, which is given by an equation considering post-buckling strength.

Punching shear capacity cannot be calculated accurately and approximated by the method for RC slabs generally. It is noted, however, that punching shear capacity of composite slabs with thin steel plate in tension side may be overestimated by the formula for RC members.

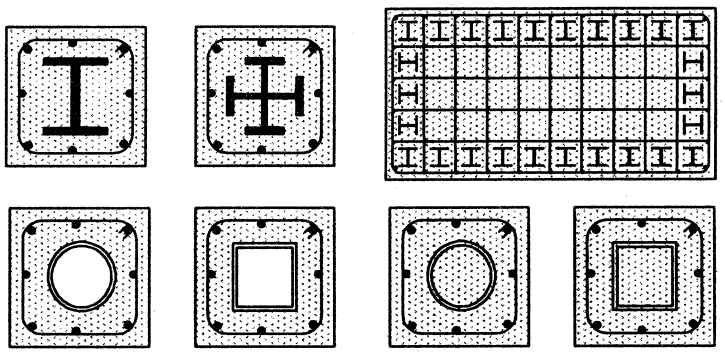

Figure 5: Typical cross sections of SRC columns

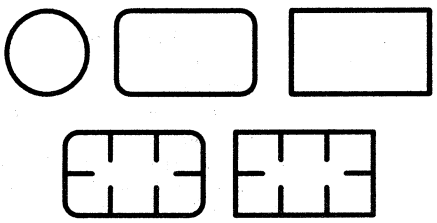

Figure 6: Typical cross sections of CFT columns

Verification methods for fatigue failure of composite slabs are provided to assure safety. At present no design formula to predict the fatigue strength of composite slabs subjected to repeated wheel loads can be provided due to lack of experimental data. Fatigue tests with simulating the passage of wheel loads are recommended for slabs in highway bridges.

5. Composite Column

The composite columns are covered by two parts such as steel reinforced concrete columns and concrete-filled tubular steel column.

- Composite columns consisting of RC and steel components, such as shaped steel, steel plate, and steel tube, embedded in concrete (SRC columns) as shown in Figure 5
- Composite columns consisting of steel tube and concrete filled fully in the tube (concrete filled steel tube, or CFT) as shown in Figure 6

The contents are the same as those included in the Parts of composite beams and slabs. The verification methods for SRC columns are fundamentally the same as those for SRC beams. The verification method for CFT columns can also be conducted in the same way as for RC except that compressive stress limit of steel tube is necessary to be reduced considering the effects of buckling.

Restorability under the effect of seismic action is particularly necessary for composite columns. The limit for localized damage to assure restorability is properly selected among the events in the process of reaching the ultimate limit state as shown in Figure 7. The damage due to yield of steel (Levels 1 and 2 in the figure) may not require any restoration work or may require light restoration work if necessary. Moderate restoration work (Level 3) is necessary after buckling. Failure of steel and crushing of concrete usually are considered to reach the ultimate limit state beyond which a great amount of restoration work or reconstruction is necessary (Level 4).

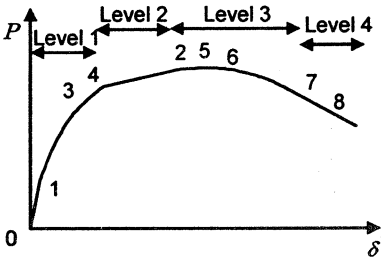

1: Point of crack generation
2: Point where concrete stress reaches its compressive strength
3: Point where steel stress reaches its yield strength
4: Yield point of member
5: Beginning of buckling of longitudinal reinforcement
6: Beginning of spalling of cover concrete
7: Point of sustained yield load
8: Point of core concrete compression fracture

Figure 7: Example of load-displacement curve and critical point of damage level

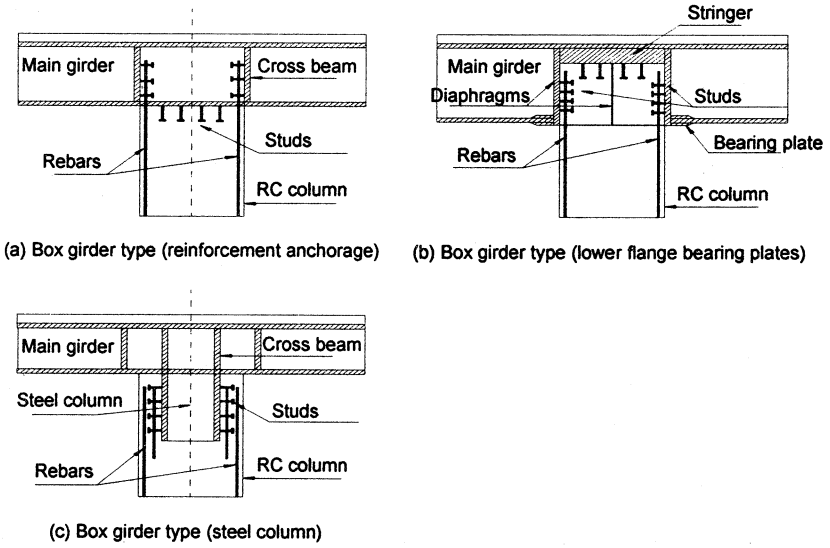

Figure 8: Typical details of joints in mixed structures

6. Mixed Structure

In the Part of mixed structures, performance requirements of members as well as joints between different types of members are provided. The typical joints between an RC column and a steel beam are shown in Figure 8. The verification of the performance requirement of members can be done according to the Parts of the composite beams, slabs, and columns in this Guidelines or relevant codes and standards for steel and RC structures. The aim of this Part is to provide verification methods for the performance requirement of joint between different types of members. In this Part, calculation models are described to analyze the behavior of joint itself and an entire structure with joints. However, it may be difficult to carry out numerical simulation around the joint because of non-linear behaviors such as cracking and separation. Therefore, unless proper techniques of numerical simulation are available to apply, the joint can be designed to be strong and rigid enough not to govern the entire behavior of mixed structures.

7. Concluding Remarks

The JSCE Guidelines for Performance Verification of Steel-Concrete Hybrid Structures is briefly introduced in this paper. Its main features are as follows:

(1) The Guidelines adopts the performance-based concept and shows verification

methods for performance requirements such as safety, serviceability, and restorability. Durability is considered for all the required performance by examining changes in performance with time.

(2) The Guidelines consists of 6 parts such as general principle, composite beam, composite slab, composite column (divided into 2 parts according to the type of composition), and mixed structure. Conventional steel-concrete composite beams, steel-concrete composite slabs, concrete filled steel tube columns, steel-concrete sandwich members, SRC members, and other new types of composite members are covered in the Guidelines.

To easily apply the concepts specified in the Guidelines to practical design work, several examples of performance verification of hybrid structures were prepared and published by JSCE[3].

ACKNOWLEGMENTS

The author would like to extend their appreciation to all the members of JSCE Joint-Committee on Steel-Concrete Composite Structure and Committee on Hybrid Structures.

REFERENCES

1. Japan Society of Civil Engineers, Guidelines for Performance Verification of Steel-Concrete Hybrid Structures, *Hybrid Structure Series* 2, 2006, (translated from the Japanese edition published in 2002).
2. International Organization for Standardization, Performance and assessment requirements for design standards on structural concrete, ISO 19338, 2003.
3. Japan Society of Civil Engineers, Examples of Performance Verification for Steel-Concrete Hybrid Structures, *Hybrid Structure Series* 1, 2006.

Ultimate Flexural Strength of Composite Beams Considering Long-term Effects

Seok Goo, Youn
Department of Civil Engineering, Seoul National University of Technology

Doobyong, Bae
School of Civil & Environmental Engineering, Kookmin University

Hyung Keun, Ryu
Department of Civil Engineering, Seoul National University

Abstract

The effects of long-term behavior of concrete slabs on the ultimate flexural strength of composite beams at positive flexure are investigated. Ultimate flexural strength of composite beam depends on crushing strain of concrete slab and the ratio of depth of plastic neutral axis and total depth of composite section. Due to long-term behavior of concrete slab, tensile stresses can be developed in the concrete slab and the compressive strength of the concrete increases also. These changes can be influenced on the ductility and the ultimate flexural strength of composite section. In this paper, long-term test of four 6.5m long steel-concrete composite beams for 400 days and ultimate load test are presented. Test results are compared with the analytical results obtained by using the age-adjusted effective modulus method (AEMM) and moment-curvature analysis. Based on the comparison, the effects of long-term behavior of concrete slab on ultimate flexural strength of composite beams are discussed.

1. Introduction

Steel and concrete composite girders are widely used for steel bridges in Korea. The steel girder is typically designed to act compositely with the concrete slab by using shear connectors to transfer shear forces between the girder and the slab. This system is most efficient in positive bending where the concrete slab is in compression. To assure ductile

behavior, composite sections should be sized to ensure sufficient yielding of steel in tension prior to concrete crushing.

Constant need for cost-effective structural forms has led to the increasing use of composite construction. In order to increase ultimate flexural strength of composite beams and maintain an economical design, higher strength steel girders or hybrid girders are used without significant increases in slab thickness. However, this decreases the ductility of composite section and can cause premature crushing of the concrete slab prior to development of the design ultimate moment capacity. In the codes of AASHTO LRFD (AASHTO 2004) and Eurocode 4 (2002), ductility requirements are specified to assure ductile behavior of composite girders and also, simplified formulas for low ductility are specified to obtain nominal flexural strength. The ductility mainly depends on the crushing strain of concrete slab and the ductility parameter represented by the ratio of the depth of plastic neutral axis and the total depth of composite section. Plastic moment capacity of composite sections can be obtained by using simple plastic theory.

Due to long-term behavior of a composite girder, the stress distribution in the composite section will be changed and thus, this can be influenced on the ductility and the ultimate flexural strength. In addition, the stress state in composite section is affected by different construction method also. In order to improve the ductility of composite girders with high strength steel girders or hybrid girders, more research works are strongly required, especially to simplify the effects of long-term behavior.

In this paper, long-term test of four 6.5m long steel-concrete composite beams for 400 days and ultimate load test are presented. To investigate the effects of creep and shrinkage of concrete slabs on composite beams, long-term behaviors such as deflections, curvatures, and strains were measured for one year. After 400 days, three specimens, which have different degrees of shear connection, were tested to get the ultimate strengths in positive moment region and another one for negative moment failure. Long-term test results were compared with the analytical results obtained by using the age-adjusted effective modulus method (AEMM). Moment-curvature analysis considering the long-term effects was also performed to estimate the theoretical ultimate strengths of the specimens. Based on the comparison of the test results and analytical results, the effects of long-term behavior of concrete slabs on the ultimate flexural strength are discussed.

2. Test specimens

2.1 Material Properties and Characteristics of specimens

Average 28 days compressive strength of concrete slab was 33MPa and average 150 days compressive strength of concrete slab was 39.5MPa. SM490 steel was used in steel girder which has yield strength of 320MPa and ultimate strength of above 490MPa. A diameter of reinforcement arranged in concrete slabs was 13mm. Four 6.5m long steel-concrete com-

posite test specimens were fabricated. Concrete slab width and thickness are 400mm and 160mm, steel girder flange width and thickness are 150mm and 9mm and web depth and thickness are 282mm and 6.5mm respectively. The ratio of longitudinal reinforcement was 0.75%. After installation of girder, casting of concrete was conducted without prop and then moisture curing was carried out during 7 days. In all specimens, distributed spacing and number of shear connection are same but a diameter of shear connection was different as 13mm, 16mm and 19mm. Thus, the degree of interaction and connection was different in each other specimen as presented in Table 1. Details of test specimens are can be shown in Fig. 1.

Table 1. Characteristics of test specimens

	SM1	SM2	SM3	HM1
Degree of shear connection	1.33	0.94	0.62	1.55
Degree of interaction	1.55	1.46	0.96	2.33
Long term test	Creep	Creep	Shrinkage	Shrinkage
Applied moment	Positive	Positive	Positive	Negative

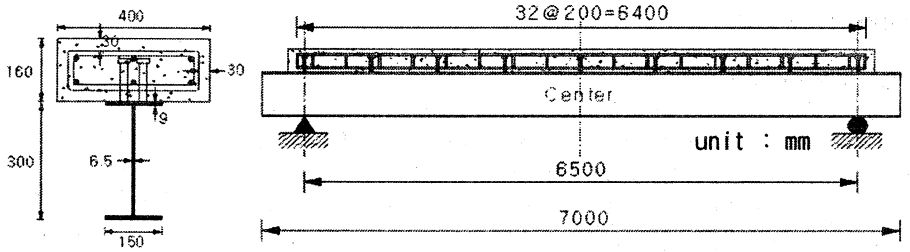

Figure 1. Details of test specimens

2.2 Measurements and loading plan

Firstly, long-term tests were conducted. In creep test specimens, SM1 and SM2, after curing of 27 day, concrete blocks were placed on the top of slab as additional dead loads as shown in Fig. 2. The weight of one block was 400N, thus 16.45N/mm distributed loads were applied. In shrinkage test specimens, SM3 and HM1, after casting concrete, the specimens were monitored continuously. The long-term behavior of all test specimens was monitored from August, 7, 2003 to August, 6, 2004 during 365 days. During the tests, deflections, strains of concrete slabs and steel girders were measured continuously.

After the monitoring, static failure tests were conducted. Loading was applied using an actuator of 490 kN capacity at the mid-span. Deflection was measured at the center of the specimens using LVDT and strain of concrete slab and steel girder were measured by several strain gauges.

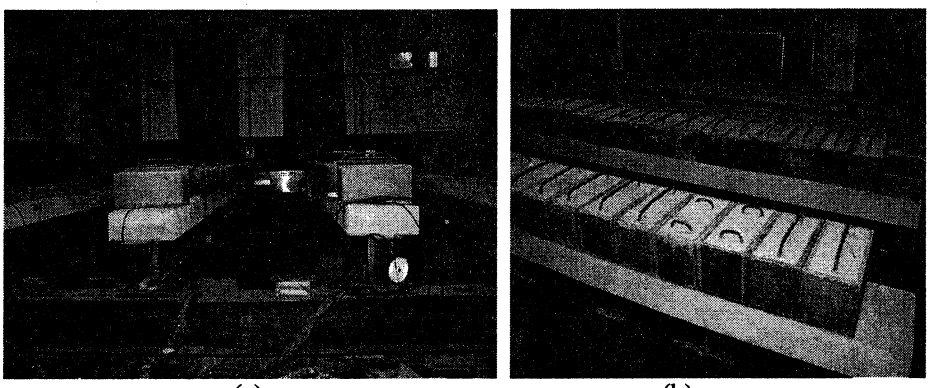

(a) (b)

Figure 2. View of creep test specimens

3. Long-term test

3.1 AEMM analysis

A simple adjustment to the effective modulus method to account aging of concrete was proposed by Trost. Later the method was more rigorously formulated and further developed by Bazant. The method is called the age-adjusted effective modulus method. The total strain at time t may be expressed as the sum of the strains produced by σ_0 (instantaneous and creep), the strains produced by the gradually applied stress increment $\Delta\sigma(\tau)$ (instantaneous and creep), and the shrinkage strain.

$$\varepsilon(t) = \frac{\sigma_0}{E_c(\tau_0)}[1+\phi(t,\tau_0)] + \frac{\Delta\sigma(t)}{E_c(\tau_0)}[1+\chi(t,\tau_0)\phi(t,\tau_0)] + \varepsilon_{sh}(t) \quad (1)$$

$$\bar{E} = \frac{E(t_0)}{1+\chi(t,t_0)\phi(t,t_0)} \text{ is the age-adjusted effective modulus} \quad (2)$$

where, $\chi(t,\tau_0)$ is called the aging coefficient and its magnitude generally falls within the range 0.6 to 0.9.

3.2 Environmental Conditions

Shrinkage of concrete was much influenced by external environmental conditions such as moisture and temperature. Thus, environmental conditions such as moisture and temperature were also monitored at the same duration continuously.

3.3 Shrinkage test results

As the time elapsed, mid-deflection of composite beam increased due to shrinkage of concrete slabs. Also, strain of composite girder was changed. Transverse cracking developed from bottom of concrete slab section to top of slab was mainly inspected. Micro transverse cracking from top to bottom slabs was also observed. Mid-deflection of composite beam and strain of concrete slab were presented in Fig. 3. In this figure, analytical curve based on AEMM using criteria of concrete in CEB-FIP was compared. In the comparison of test results with analysis for steel girder, the effect of temperature variation could not be neglected. Thus, temperature compensation had been conducted.

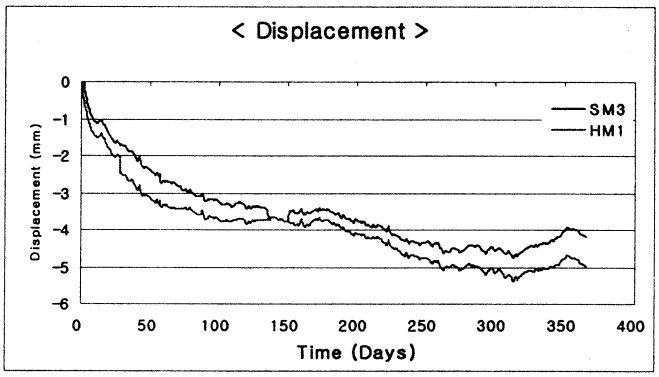

(a) Deflection

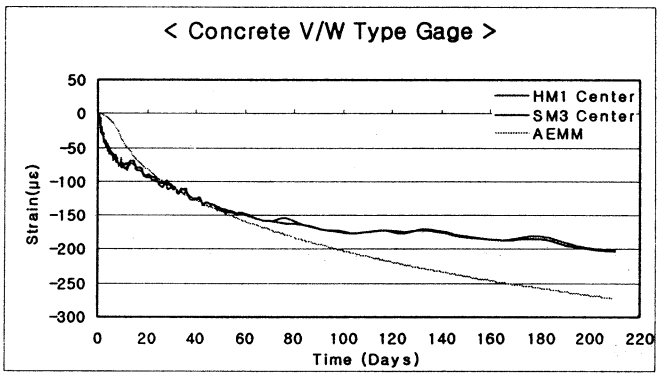

(b) Strain of concrete slab

Figure 3. Long-term monitoring of Shrinkage test specimens

3.4 Creep test results

Similarly, as the time elapsed, mid-deflection of composite beam increased due to creep of concrete slabs. Also, strain of concrete slab was changed. Transverse cracking developed from bottom of concrete slab section to top of slab was similarly investigated. Mid-deflection of composite beam and strain of concrete slab were presented in Fig. 4. In this figure, analytical curve based on AEMM using criteria of concrete in CEB-FIP was compared. In the comparison of test results with analysis, the temperature compensation was also included.

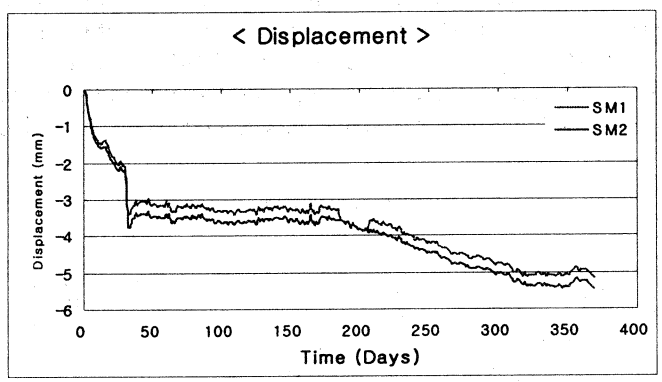

(a) Deflection

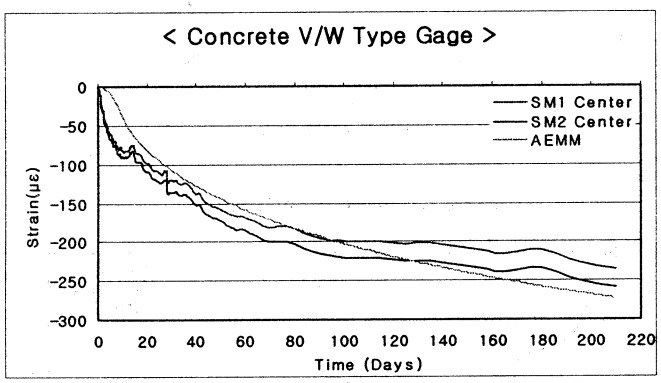

(b) Strain of concrete slab

Figure 2. Long-term monitoring of Creep test specimens

4. Static load test

4.1 Ultimate strength

All the test specimens were failed with showing ductile behaviors and in cases of posi-

tive bending test specimens were failed with showing crushing of top-fiber concrete slabs as shown in Fig. 5. From the failure tests, load-deflection curves were obtained as shown in Fig 6. In this figure, displacements of uncracked and cracked composite beams were evaluated and compared with the test results. Ultimate loads of the specimens calculated by simple plastic analysis with 33MPa of concrete compressive strength were estimated as 220.92kN for the positive moment test specimens and 140.31kN for the negative moment test specimen. Ultimate loads of the composite beams were presented in Table 2. From the Table 2, it is confirmed that ultimate loads for all specimens were higher than the calculations, although the SM2 and SM3 was designed as partial shear connection composite beams (Table 1). Since, design strength equation of stud shear connection is based on the push-out tests and bond and friction between slab and girder were neglected, it is considered that degree of shear connection was evaluated conservatively for the composite beams.

(a) SM1

(b) SM2

(c) SM3

(d) HM1

Figure 5. View of test specimens after failure

Table 2. Failure test results of composite beams

	SM1	SM2	SM3	HM1
Collapse Load	271.46 (kN)	251.86 (kN)	245 (kN)	145.92 (kN)
Ultimate load ratio	1.23	1.14	1.11	1.04

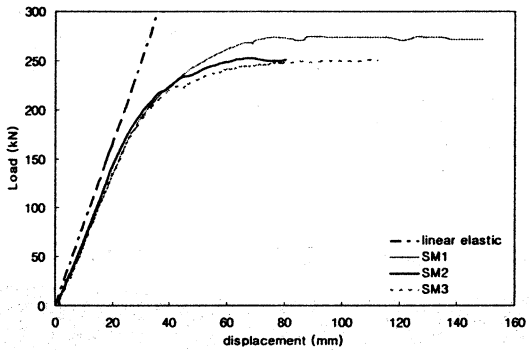

(a) Positive moment

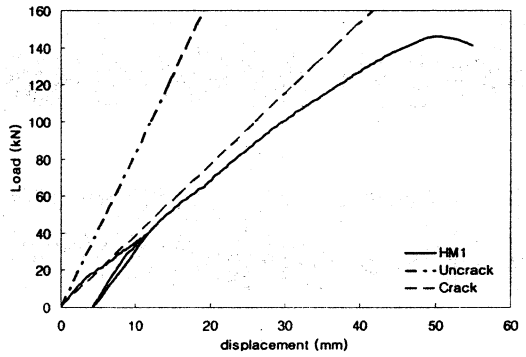

(b) Negative moment

Figure 6. Load-deflection curve of composite beams

In the test specimens, it was intended that shear connections were installed to achieve full or partial shear connections as presented in Table 1. Load-relative slip curves were also measured experimentally through the static loading test performed up to collapse (Figure 4). Maximum slips were measured by 1.1mm (Fig. 7). From this result, it is considered that the test specimen could be assumed as the full composite section until the collapse.

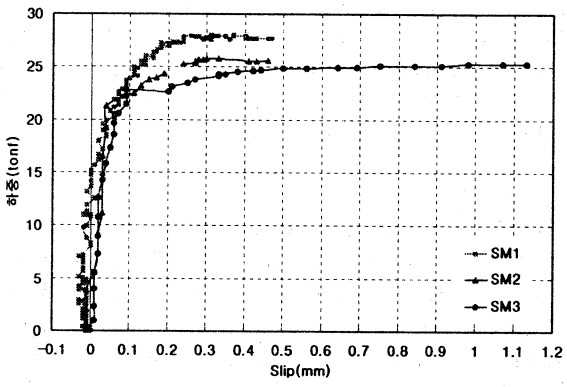

Figure 7. Load-relative slip curve

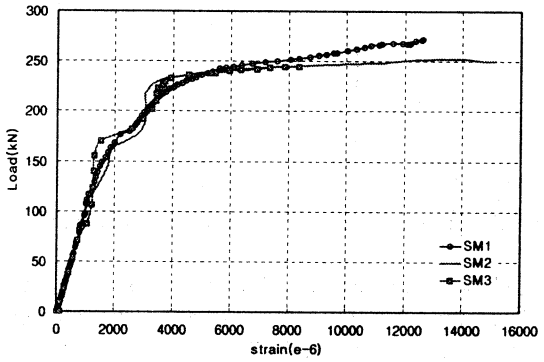

(a) Positive moment

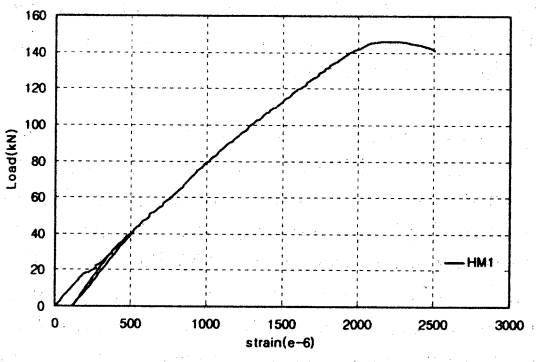

(b) Negative moment

Figure 8. Strain of bottom flange in composite beams

Strain of bottom flange was measured with increased load as presented in Fig 8. Maximum strain happened at bottom flange for all test specimens. Fig. 8 plots the maximum strains (strain at the bottom flange) in the maximum positive moment section and in the negative moment section of the girder measured until the failure. From the level of the developed strains, yielding load could be assumed.

4.2 Moment-curvature analysis

In order to estimate the ultimate strength of composite beam of SM1, moment-curvature analysis was conducted. The stress-strain curve of steel is assumed as an elastoplastic stress-strain curve and the stress of concrete slab is obtained by ACI method. The average compressive strength of concrete slab is used as 33MPa at 28 days and 39.5MPa at 150days which are obtained by previous material tests. The yield strength of steel girder is assumed as 320MPa. Concrete crushing strains are assumed as 0.003 and 0.0035.

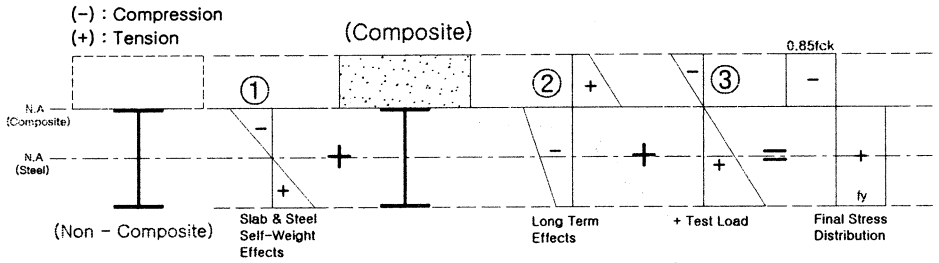

Figure 9. Stresses developed in composite beams at each construction phases

Ultimate strengths of SM1 for six conditions obtained by moment-curvature analysis are presented in Table 3. From the comparison of the ultimate strengths in the Table 3, concrete strength affects on the ultimate strength. But concrete crushing strain does not influence significantly. It is considered that this result can be affected by the assumption of elastoplastic stress-strain curve for steel girder and low ductility parameter ($D_p / D_t =$ 0.23) of SM1. If ductility parameter is decreased and strain hardening is considered, ultimate strength will be affected by crushing strain.

In case of considering stresses at each construction phases as shown in Fig. 9, the ultimate strength increases although 33MPa of concrete compressive strength used in the analysis and hence, the difference to test result is reduced significantly. In the analysis, initial stress state caused by dead load and long-term behavior of composite section is considered. If concrete compressive strength of 39.5MPa is used, the ultimate strength will be increased about 15.6MPa based on the comparison of conditions of (1) and (2), and the difference will be reduced significantly. Fig. 10 shows F.E. model for SM1 which was modeled for confirming the results of moment-curvature analysis and Fig. 11 represents the relationship between the applied load and the tensile strain of bottom

flange. From the Fig. 11, it can be found that the ductility of the case of considering long-term effects of composite girders is larger than that of neglecting long-term effects.

Table 3. Ultimate strength of SM1 obtained by moment-curvature analysis

Conditions	Ultimate strength	Difference to test result of SM1
(1) $\varepsilon_{cu} = 0.003$, fcm = 33MPa	220.0kN	50.56 kN
(2) $\varepsilon_{cu} = 0.003$, fcm = 39.5MPa	235.6kN	38.46 kN
(3) $\varepsilon_{cu} = 0.0035$, fcm = 33MPa	222.8kN	48.66kN
(4) $\varepsilon_{cu} = 0.0035$, fcm = 39.5MPa	237.3kN	34.16kN
(5) Construction phases, fcm = 33 MPa neglecting reinforcements	240.1KN	31.41 kN
(6) Construction phases, fcm = 33MPa considering reinforcements	247.0kN	24.41 kN

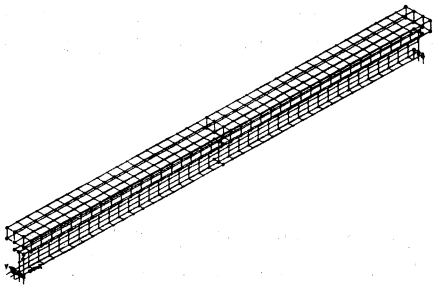

Figure 10. Finite element model for SM1

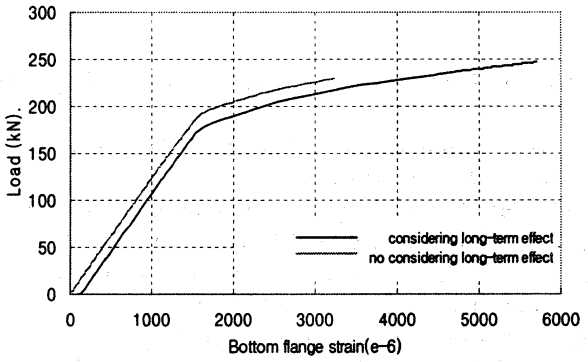

Figure 11. Relationship between applied load and tensile strain of bottom flange

5. Conclusion

In this paper, long-term test of four 6.5m long steel-concrete composite beams for 400 days and ultimate load test are presented and test results are compared with the analytical results obtained by using the age-adjusted effective modulus method (AEMM) and moment-curvature analysis. Based on the comparison, the effects of long-term behavior of concrete slab on the ultimate flexural strength of composite beams are discussed.

Long-term behaviors of composite beams give positive effects on the bending capacity and the ductility of composite beams. So, if bridge engineer calculate bending capacity according to current bridge design code based on strength design method, at least there is no need to consider long-term effects of composite girders. In case of strength evaluation, long-term effects can be considered for composite girders.

If the effects of long-term behavior of concrete slab on the ultimate flexural strength of composite beams are included in design codes, it is possible to maintain an economical design for composite bridges with high strength steel girders and hybrid girders also. In order to obtain these advantages, more research works will be strongly required and simplified formula for evaluating the ultimate strengths of composite beams should be developed.

6. Acknowledgement

This study is supported by a **Korea Bridge Design & Engineering Research Center**. The authors would like to thank the **Korea Bridge Design & Engineering Research Center**.

7. Reference

1. AASHTO, *AASHTO LRFD Bridge Design Specifications*, 3rd Ed., 2004, Washington, D.C.
2. Ansourian, P., "Plastic rotation of composite beams," *Journal of Structural Division*, ASCE, Vol. 108, No. 3, 1982, pp. 643-659.
3. Bazant, Z.P., 1972, Prediction of concrete creep effects using age-adjusted effective modulus method, Proceedings, *ACI Journal*, Vol.69, 212-217
4. Bradford M.A., 1997, Shrinkage behavior of steel-concrete composite beams, *ACI, Structural Journal*, Vol.94, No.6, Nov.-Dec., 625-632
5. CEB, 1991, *CEB-FIP Model Code 1990*, Final Draft, July
6. Deric J. Oehlers, Ninh T. Nguyen, Marfique Ahmed, M.A.Bradford, 1997, Partial Interaction in Composite Steel and Concrete Beams with Full Shear Connection, *J.*

Const. Steel Res., Vol.41, No. 2/3, 235-248
7. Eurocode 4: *Design of Composite Steel and Concrete Structures, Part 1.1, General rules and rules for buildings*, prEN 1994-1-1:2002(E), 2002.
8. Gilbert, R.I., 1989, Time-dependent analysis of composite steel-concrete sections, *Journal of Structural Engineering,* ASCE, Vol.115, No.11, Nov., 2687-2705
9. Mans, P., Yakel A.J., and Azizinamini, A., "Full-scale testing of composite plate girders constructed using 485-MPa high-performance steel," *Journal of Bridge Engineering*, ASCE, Vol. 6, No. 6, 2001, pp. 598-604.
10. Trost, H, 1967, Auswirkungen des Superposition-sprinzips auf Krech und Relaxations Probleme bei Beton und Spannbeton, *Beton und Stalbetonbau*, Vol.62, No.10, 230-238
11. Wittry, D.M., "An analytical study of the ductility of steel-concrete composite sections," MS thesis, University of Texas-Austin, 1993.
12. Yakel, A., and Azizinamini, A., "Improved moment strength prediction of composite steel plate girders in positive bending," *Journal of Bridge Engineering*, ASCE, Vol. 10, No. 1, 2005, pp. 28-38.

EXPERIMENTAL STUDIES ON STRESS TRANSMISSION BEHAVIOR BETWEEN STEEL AND CONCRETE IN HYBRID STRUCTURE

Akinori NAKAJIMA

Utsunomiya University, Japan

Abstract

Nowadays, steel-concrete hybrid members and structures are widely used in the various bridge structures. In these structural systems, it is important to ensure the required stress transmission between the steel member and the concrete one, and it is necessary to arrange the various shear connectors adequately. Furthermore, it is required to establish the comprehensive design method taking into account the stress transmission behavior between steel and concrete.

Against the background of these research needs, some research works focusing on the behavior of the stud shear connector and the bond between the steel plate and the concrete are introduced in this paper. First, the static strength and fatigue strength of the stud under the alternating load condition as well as the pulsating load condition is investigated by employing the devised push-pull test specimen. Second, the strain behavior of the stud base is investigated by employing the pipe stud with the inside strain gages near the base in order to observe the strain behavior at the base of the stud shank. Finally, the bonding behavior between steel and concrete is investigated by employing the small scale push-out test under the constant bearing stress.

1. Introduction

Nowadays, steel-concrete hybrid structures are widely used in the various bridge structures and members. The composite girder which is composed of the steel girder and the concrete slab, the composite slab which is composed of the concrete slab and the bottom steel plate, and the composite column which is composed of the steel tube and the infilled concrete are the popular steel-concrete hybrid structural members. Moreover, various types of bridge structures with steel-concrete hybrid members such as the prestressed concrete bridge with corrugated steel web plate, the mixed rigid frame bridge in which the steel girder is rigidly connected to the reinforced concrete pier, and the mixed girder bridge and the mixed cable-stayed bridge in which the steel girder is longitudinally connected to the prestressed concrete girder are constructed in Japan.

For example, in the continuous steel-concrete composite girder, the cracking of the concrete slab in the vicinity of the intermediate support is an important problem to be solved up to now. From the viewpoint of serviceability, durability and constructability, a design method to admit the controlled crack width for the composite girder with not prestressed concrete slab is proposed[1)]. The design method which requires to predict the precise crack width and the strain distribution of the reinforcing bars is also developed[2)]. Furthermore, the researches focusing on the behavior of the various shear connectors, and the bond between the concrete slab and the flange of the steel girder are conducted actively.

On the other hand, the mixed rigid frame bridge in which the bearings are omitted between the steel girder and the reinforced concrete pier can increase the seismic performance of the bridge and can reduce the maintenance cost. The mixed girder bridge and the mixed cable-stayed bridge have the features that the bridge system can restrict the negative reaction by employing the center span with the lighter steel girder instead of the heavier concrete girder. In these structural systems, it is important to ensure the required stress transmission between the steel member and the concrete one and to arrange the various shear connectors adequately. Furthermore, it is required to establish the comprehensive design method taking

into account the stress transmission behavior between steel and concrete.

From this background, some researches focusing on the behavior of the stud shear connector and the bond between the steel plate and the concrete are introduced in this paper. In the steel-concrete mixed rigid frame bridge, the studs located at the connection between the steel girder and the reinforced concrete pier are subjected to the alternating shear force during earthquake excitations. However, in a conventional push-out test such as the one specified in the Japanese standard push-out test method[3], the only pulsating shear force can be applied to the stud. Thus the static strength and fatigue strength of the stud have not been investigated under the alternating load condition by employing this type of push-out test method[4),5].

In this case, since the static and fatigue failures of the stud usually occur at the base of the stud shank, it can be predicted that the base of the stud shank is subjected to large strain response. Therefore, it is important to observe the strain behavior at the base of the stud shank in order to know the stress concentration near the base and the shear force transferred through the stud shank. However, it is difficult to measure the strain response at the base of the solid stud shank by experiment because of the welding at the base and the coating necessary to protect the strain gages. Then, pipe stud shear connectors are introduced instead of ordinary solid studs for measuring the strain behavior at the base of the stud shank[6]. In this case, strain gages are installed inside the pipe stud near the shank base where the gages are able to measure the base strain response successfully.

Furthermore, in these steel-concrete hybrid structures, there are many contact surfaces between steel and concrete, and it is required to transfer the stress adequately from steel to concrete or vice versa. Therefore, in order to clarify the structural behavior of the steel-concrete hybrid structure rationally, it is required to know the stress transmission behavior due to the normal stress and the shear stress at the contact surface between steel and concrete[7]. Here, the push-out test specimen which is composed of the steel plate sandwiched between two concrete blocks is carried out to investigate the bonding behavior of the contact surface be-

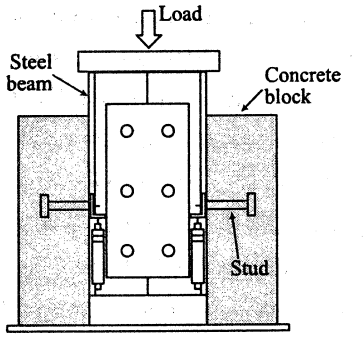

Fig. 1 Conventional push-out test specimen

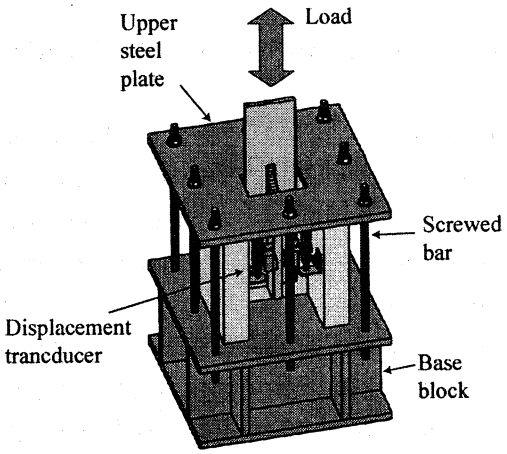

Fig. 2 Push-pull test specimen

tween steel and concrete under the monotonic shear force and the constant bearing force[8].

2. Stud behavior under alternating load

Fig. 1 shows the conventional push-out test specimen such as the one specified in the Japanese standard push-out test method[3] to investigate the shear strength of the stud shear connector. The only one-sided shear force can be applied to the stud. On the other hand, **Fig. 2** shows the test specimen employed in this research. The alternating load as well as the pulsating load is applied to the specimen by clamping the top of the steel plate at the head of the loading actuator. In this paper, the load condition with only compressive shear force cycles or only tensile shear force cycles is defined as the pulsating load condition and the reversed cyclic shear force is defined as the alternating load condition.

2.1 Outline of specimen

The proportion of the specimen shown in **Fig. 2** is determined so that the alternating shear force can be applied easily to the specimen. A pair of studs of 13mm diameter and 100mm high are arranged on one side of the steel plate of 530mm • •

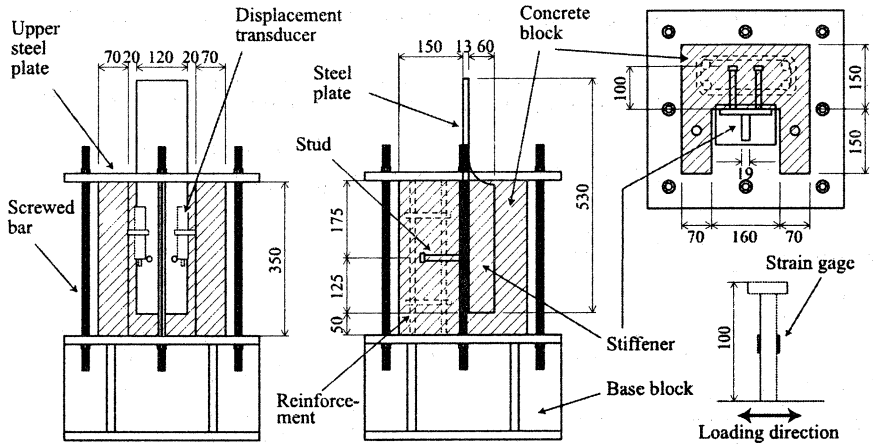

Fig. 3 Proportion of specimen

120mm• •13mm as shown in **Fig. 3**. The plate is stiffened by another longitudinal steel plate welded on the other side so that the plate should not buckle during the application of the load. The concrete block has a concave section as shown in **Fig. 3** so that the specimen should not rotate in applying the load to the steel plate. Four 10mm diameter longitudinal deformed bars and two 6mm diameter stirrups of 200mm spacing are provided to protect the premature cracks in the concrete block. In applying the load, the concrete block is inserted between the steel base block and the upper steel plate, and is fixed by eight screwed bars as shown in **Fig. 2**. Two displacement transducers are installed to measure the relative slip between the concrete block and the steel plate at the level of the stud shown in **Fig. 3**. A pair of strain gages is also placed on the surface of the each stud shank at its midheight to observe the strain behavior of the studs qualitatively. Here, the test is conducted by employing three series of specimens which differ in material properties of the concrete and stud as shown in **Table 1**.

2.2 Test procedure

(1) Static loading test

In each series, two specimens are tested under the pulsating and alternating loading programs respectively in order to investigate the shear force-relative slip behavior

Table 1 Number of specimen, loading condition and material property

Test series		Number of specimen		Concrete strength (N/mm^2)	Yield strength of stud (N/mm^2)
		Pulsating	Alternating		
Static test	Series A	2	2	37.1	311
	Series B	2	2	43.5	360
	Series C	2	2	40.1	371
Fatigue test	Series A	15	10	37.1	311
	Series B	8	8	43.5	360
	Series C	4	6	40.1	371

of the stud and its maximum strength. In the pulsating load condition, one-sided loading cycles are repeated twice up to the peak load and the peak load is increased up to failure of the specimen. On the other hand, in the alternating load condition, fully reversed loading cycles are repeated up to the peak load and the peak load is increased up to the failure of the specimen. During the loading program, the magnitude of the load, the relative slip and the strain of the stud are measured by the data logger at each loading step. The load increment is set to one-fifth to one-tenth of each peak load.

(2) Fatigue loading test

In the fatigue test, a set of the maximum and the minimum load is changed in order to apply the required amplitude of the shear force to the stud. In Series A, the wide range of the shear force amplitude from 15 to 60kN with the loading frequency of 3Hz is applied to one stud. In Series B, the comparatively large shear force amplitude from 25 to 50kN with the loading frequency of 3Hz or 0.1Hz is applied to one stud. On the contrary, in Series C, the shear force amplitude to one stud varies from 10 to 45kN with the loading frequency of 3Hz. Constant minimum load of 2.5kN is applied to the specimen under the pulsating load condition. Equal magnitude of the maximum and minimum load is set under the alternating load condition. During the fatigue test, the magnitude of the load, the relative slip and

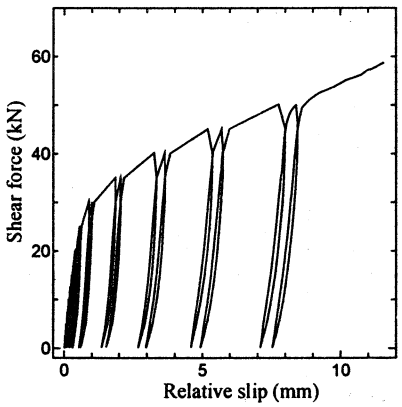

Fig. 4-a Pulsating load condition

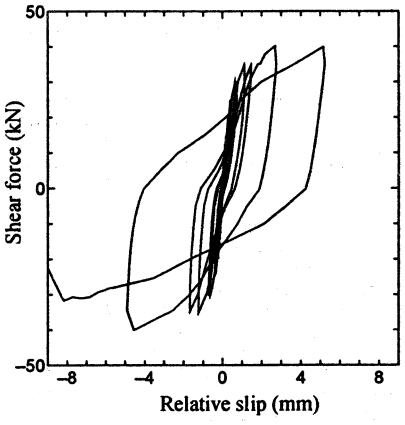

Fig. 4-b Alternating load condition

Fig. 4 Relation between shear force and relative slip

the strain of the stud are measured by the dynamic data acquisition system at each 10s to 600s taking the expected fatigue life of each specimen into consideration.

2.3 Test results

(1) Static loading test

The typical examples of the relation between the shear force and the relative slip obtained through the pulsating and alternating static tests are shown in **Fig. 4**. The ordinate is the shear force applied to one stud and the abscissa is the average value of the relative slip between the concrete block and the steel plate measured by two displacement transducers. According to these figures, there is a difference between the overall shape of the shear force-relative slip relation under the alternating load condition and the one under the pulsating load condition, although one-sided envelopes up to about 2mm under the both load conditions appears similar. The shear force-relative slip relation curve under the pulsating load condition in **Fig. 4-a** resembles the typical one obtained from the standard push-out test for the stud. On the other hand, the shear force-relative slip relation under the alternating load condition **Fig. 4-b** resembles the so-called slip-model relation in shape. In this case, the shear force is considered to be transmitted by the bearing force between the concrete and the stud in the transverse direction

Table 2 Summary of static test results

Type of specimen	Maximum strength (kN)	Yield strength (kN)	Shear stifness (N/mm)	Concrete strength (kN/mm^2)
Series A (Pulsating)	57.7	27.5	53.3	37.1
Series A (Alternating)	42.6	24.7	117.3	
Series B (Pulsating)	59.8	38.3	129.5	43.5
Series B (Alternating)	49.1	26.1	127.4	
Series C (Pulsating)	56.6	34.2	71.3	40.1
Series C (Alternating)	44.5	27.3	75.1	
Average of Pulsating	58.0	33.3	84.7	40.2
Average of Alternating	45.4	26.0	106.6	
Conventional push-out test	54.2	30.1	82.7	34.6

to its shank. A gap occurs between the surface of the stud and the surrounding concrete near its base under the alternating load condition. Therefore, the shear force-relative slip relation under the load condition shows this kind of shape. The above relation between the shear force and the relative slip is useful for analyzing the responses of the stud in the hybrid structure under the earthquake motion.

Table 2 summarizes the maximum shear strength, the yield shear strength and the shear stiffness of each type of the specimen. The shear stiffness is defined as the slope of the secant at the point where the shear strength is one-third of the maximum shear strength on the shear force-relative slip relation. The yield shear strength is defined as the point where 0.2mm offset of the slip parallel to its shear stiffness crosses the shear force-relative slip relation. According to the definition, the average maximum shear strength and the yield shear strength under the pulsating load condition are about 28% larger than those under the alternating load condition when the average value of all data is used. This is the reason why the shear strength under the alternating load condition is considered to be affected

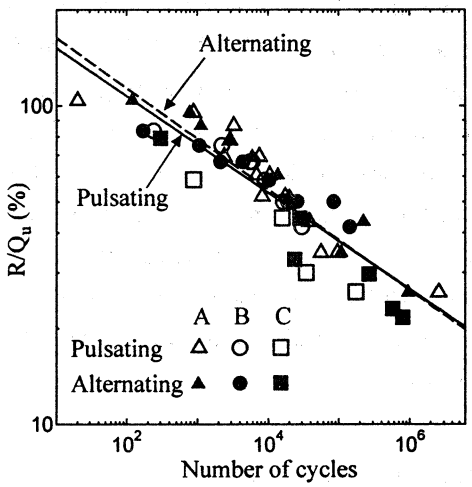

Fig. 5 Relation between R/Q_u and number of repetition of shear force

by the low cycle fatigue of the stud. However, the maximum shear strength and the yield shear strength under the alternating load condition are larger than the ones under the pulsating load condition, since the maximum shear strength under the alternation load condition becomes double to the one sided amplitude considering the maximum amplitude of the applied shear force. On the other hand, it is observed that the shear stiffness in Series B is significantly larger than the one in other series because the compression strength of concrete in Series B is larger than the one in other series. It is also observed that the shear stiffness under the alternating load condition is almost same as the one under the pulsating load except for Series A. For reference, the shear strength, the yield strength and the shear stiffness of the stud of 13mm diameter and 70mm high under the conventional push-out test is also shown in **Table 2**. These properties are almost same as those by the test conducted here.

(2) Fatigue loading test

Fig. 5 shows the S-N diagrams for all the test results obtained from Series A, B and C. The ordinate is the amplitude of the shear force applied to one stud and the abscissa is the number of the repetition of the shear force up to the fatigue failure of the specimen. There is a difference between the maximum shear

strength in each series shown in **Table 2** due to the difference in material properties in each series. Therefore, the amplitude of the shear force normalized by the each maximum shear strength under the pulsating load condition is taken in the ordinate. Moreover, two regression lines are shown in **Fig. 5** by the solid line and the dashed line for the results under the pulsating and alternating load conditions, respectively. According to the both regression lines for the alternating and pulsating load conditions, there is little difference between the fatigue strength characteristics under the both load conditions. As a result, while the slope of the regression line for the alternating load condition is evaluated as 6.3, that for the pulsating load condition is evaluated as 6.6.

3. Strain behavior of stud base

Since the static and fatigue failures of the stud usually occur at the base of the stud shank, it can be predicted that the base of the stud shank is subjected to large strain response. Therefore, it is important to observe the strain behavior at the base of the stud shank in order to know the stress concentration near the base and the shear force transferred through the stud shank. Here, pipe stud shear connectors are introduced to the push-pull specimen instead of ordinary solid studs for measuring the strain behavior at the base of the stud shank.

3.1 Outline of specimen

The experimental setup of the push-pull test specimen with a pair of pipe studs is similar to the one employed in the previously explained research shown in **Fig. 2**. The pipe studs have an inside diameter 17.9mm, outside diameter 21.7mm and height 120mm, and are arranged on the base plate as shown in **Fig. 6**. The base plate has dimensions of 530mm × 120mm × 13mm as shown in **Fig. 6-a**. The pipe studs are embedded through the opening in the base plate and welded from the outside of the pipes as shown in **Fig. 6-b**. The procedure of the load application is also same as the one in the previously explained research.

One pair of strain gages is installed at the base and another pair at the midheight of each pipe stud, as shown in **Fig. 6-b**. The inside area of the pipe stud is filled

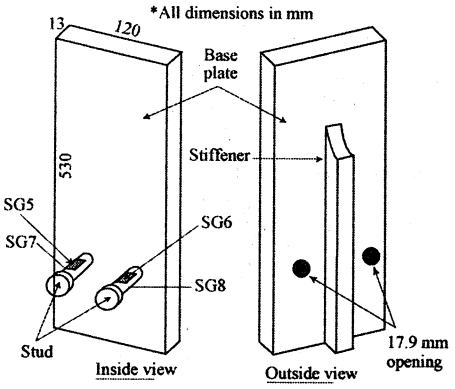

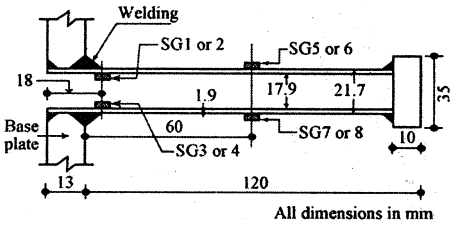

Fig. 6-a Base plate with studs and stiffener

Fig. 6-b Pipe stud with strain gages

Fig. 6 Strain gage locations on stud shank

by cement mortar to minimize the local deformation of the pipe section during the tests. Anyway, the pipe stud is only used for the experimental research and is not used in the actual structures.

3.2 Test procedure

A series of experiments is carried out on a total of twenty-one push-pull test specimens. Here, the behavior of the pipe studs is investigated under the condition of the pulsating and alternating loading as well as the monotonic loading. The pulsating compressive or tensile loading cycles are repeated with several incremental peak loads up to 80 kN, and then the load is increased monotonically up to the failure of the specimen. On the other hand, complete reversal loading cycles (from compression to tension or vice versa) are repeated up to the failure of the specimen under the alternating load condition. Moreover, the monotonic compressive or tensile load is applied to the specimen under the monotonic load condition. During the application of the load, the relative slip between the concrete block and the base plate, and the strain at the base and midheight of the stud shank are measured at each loading step.

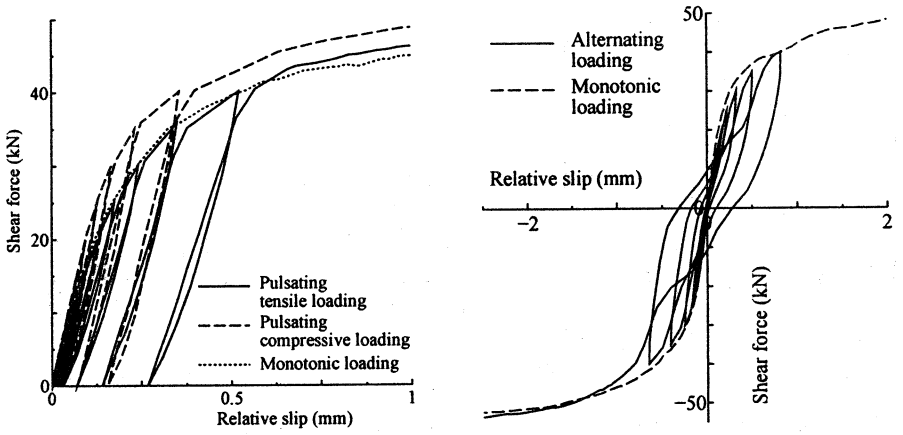

Fig. 7-a Pulsating load condition **Fig. 7-b** Alternating load condition

Fig. 7 Relation between shear force and relative slip

3.3 Test results

(1) Shear force-relative slip relations

The typical shear force-relative slip relation under the pulsating load condition is shown in **Fig. 7-a**. The ordinate indicates the shear force applied to one stud and the abscissa indicates the average value of the relative slip between the concrete block and the base plate. The relative slip is recorded by the two displacement transducers installed on both sides of the stiffener, and the average value is used in the shear force-relative slip relation. The absolute values of the shear force and relative slip are taken for the compressive loading. The relations between the shear force and relative slip under the alternating compressive loading for the pipe stud is shown in **Fig. 7-b**. These relations are also compared with the one under the monotonic load condition, and the envelope curves of the relations under the both load conditions almost agree with the curve under the monotonic load condition. Furthermore, the outlines of these relations are also similar to the ones for the solid stud as shown in **Fig. 4**.

(2) Strain behavior of the stud shank

The major focus of the experimental investigation is the strain behavior at the base and midheight of the stud shear connectors under three different types of loading. The typical relations between the shear force per stud and the direct

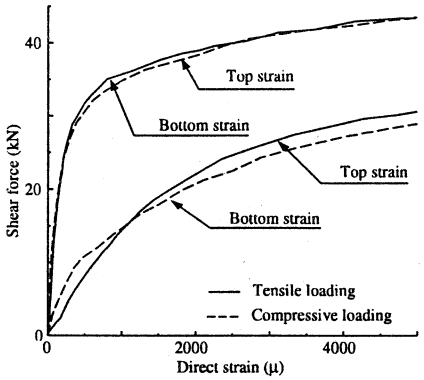

Fig. 8-a At base

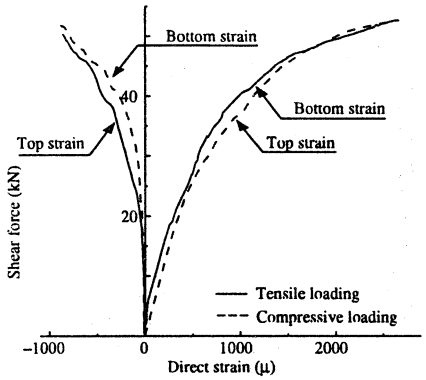

Fig. 8-b At midheight

Fig. 8 Relation between shear force and direct strain under monotonic load condition

strain at the base and midheight under the monotonic load condition are shown in **Fig. 8**. In this figure, the absolute value is taken as the negative of the shear force only under compressive loading, and the top and bottom strain at the base and the midheight corresponds to the location of the strain gages shown in **Fig. 6-b**.

For compressive loading, at the base the magnitude of the bottom-side strain is greater than that of the top-side strain with the same sign, while at the midheight, the top-side strain is greater than the bottom-side strain with the different sign as shown in **Fig. 8**. The opposite behavior is observed for the monotonic tensile loading.

On the basis of elementary beam theory, the axial strain as well as the bending strain is determined from the direct strain of the stud shank. The bending strain at any section is one-half the difference between the top and bottom strains, whereas the axial strain is the average of the top and bottom strains. The axial strain and bending strain relations at the base and midheight under monotonic tension and compressive loadings are shown in **Fig. 9**. The axial strain as well as the bending strain at the base is much larger than the strains at the midheight, and the sign of the curvature at the base is opposite that at the midheight. Moreover, the axial

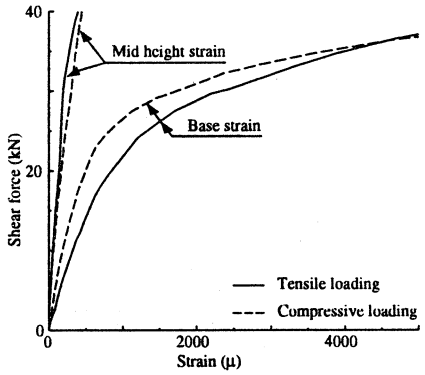

Fig. 9-a Axial strain

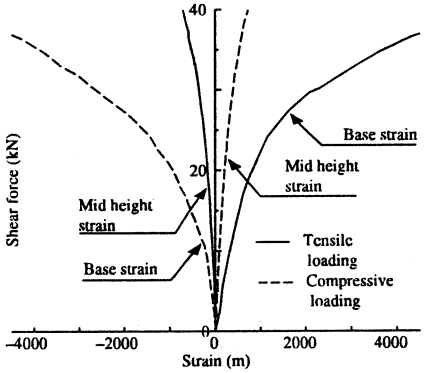

Fig. 9-b Bending strain

Fig. 9 Relation between shear force and axial and bending strain under monotonic load condition

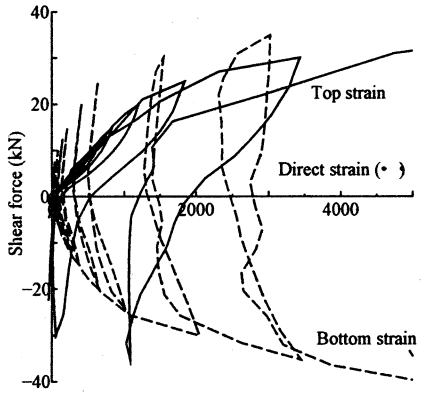

Fig. 10-a At base

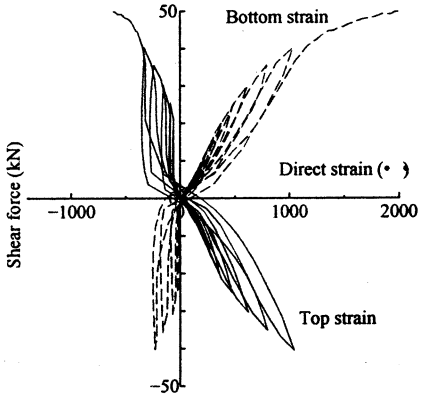

Fig. 10-b At midheight

Fig. 10 Relation between shear force and direct strain under alternating load condition

strain has always tensile strain irrespective of the loading direction.

Fig. 10 shows the typical shear force-direct strain relations at the base and midheight of the stud shank under the alternating load condition. The solid line in **Fig. 10** is the shear force-direct strain relation at the top strain and the dashed line is the one at the bottom strain. The shear force-direct strain relations at the base is totally different from the same strain relation at the midheight. Namely,

the strains at the base are always tensile ones, while the strains at the midheight become tensile and compressive ones alternately dependent on the direction of the load. This is the reason why the axial strain at the base in **Fig. 10-a** is much larger than the one at the midheight in **Fig. 10-b**.

4. Interface bonding behavior between steel and concrete

It is important to clarify the stress transfer mechanism through the contact surface between steel and concrete in steel-concrete hybrid structures. Here, the bonding behavior of the contact surface between steel and concrete under the bearing stress is investigated by conducting the push-out test.

4.1 Outline of specimen

In this research, the push-out test specimen which is composed of the steel plate and two concrete blocks on its both sides are employed and the static push-out test is conducted by applying the shear force to the contact surface under the constant bearing force as shown in **Fig. 11** and **Fig. 12**. Since the concrete is placed abut on the upright steel plate, the natural bond may be produced between the steel plate and the concrete. **Fig. 12** shows the proportion of the specimen. The bearing force is applied to the contact surface by fastening four screwed bars with 20mm diameter through the outside steel plates with holes. Each screwed bar is fastened with almost equal tensile force by using the torque wrench and the bearing force is measured by the load cell as shown in **Fig. 11**. The bearing stress is defined as the bearing force normalized by the contact area between the steel plate and concrete. In this case, three different magnitude of the bearing stress as 0.4, 1.0 and 2.0 N/mm^2 are applied to the specimen, and 2 specimens are employed for the push-out test under each magnitude of the bearing stress. The average compressive strength of the concrete during the test is 33.1 N/mm^2. The grade of the central steel plate is SS400 and its surface is covered by the general anti-corrosion coating.

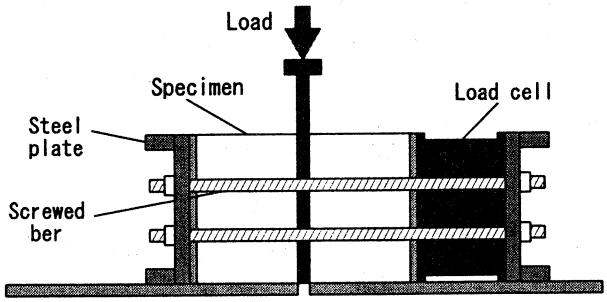

Fig. 11 Outline of specimen

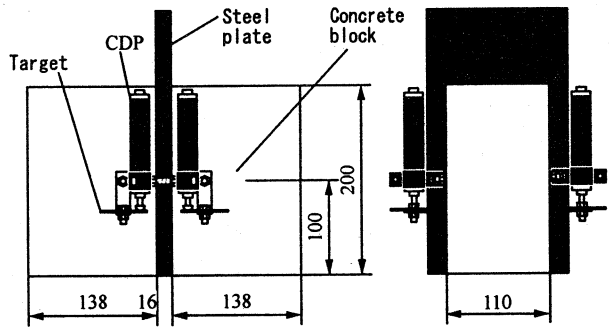

Fig. 12 Proportion of specimen (Dimensions in mm)

4.2 Test procedure

The static testing machine is employed for the push-out test. Two steel plate is arranged on the loading bed with 20mm gap and the specimen is placed on the steel plates as shown in **Fig. 11**. The contact surface between the central steel plate and the concrete blocks is subjected to the shear stress by applying the vertical load to the top of the central steel plate under the condition that the constant bearing force is applied to the surface normally. Four displacement transducers with the division of 1/1000mm are installed to measure the relative slip between the central steel plate and the concrete blocks during the push-out test as shown in **Fig. 12**.

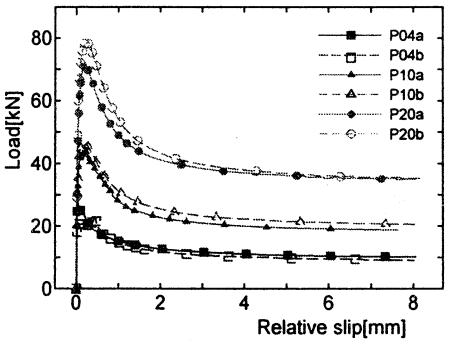

Fig. 13-a Normal scale

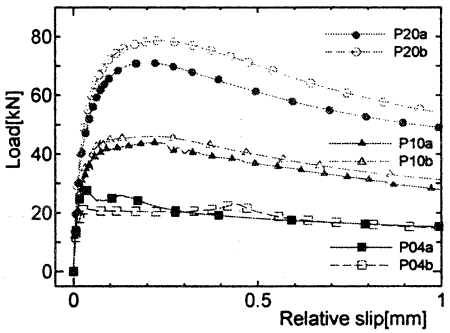

Fig. 13-b Scale-up

Fig. 13 Relation between vertical load and relative slip

Table 3 Results of push-out test

Specimen	Maximum shear stess (N/mm^2)	Slip at maximum load (mm)	Residual shear stress (N/mm^2)	Slip at residual load (mm)
P04a	0.628	0.032	0.234	7.534
P04b	0.524	0.443	0.219	7.526
P10a	0.998	0.223	0.429	7.531
P10b	1.047	0.217	0.471	7.555
P20a	1.617	0.201	0.801	7.547
P20b	1.787	0.231	0.807	7.572

4.3 Test results

(1) Push-out test

Fig. 13 shows the relations between the applied vertical load and the relative slip including the scale up relations within 1mm slip. The ordinate shows the applied vertical load and the abscissa shows the relative slip between the central steel plate and the concrete block. The marks and the lines correspond to the variation of the bearing stress such as 0.4, 1.0 and 2.0 N/mm^2. According to these figures, the relative slip is found to be very small up to the maximum load. When the applied load goes beyond the maximum load, the applied load decreases rapidly with the

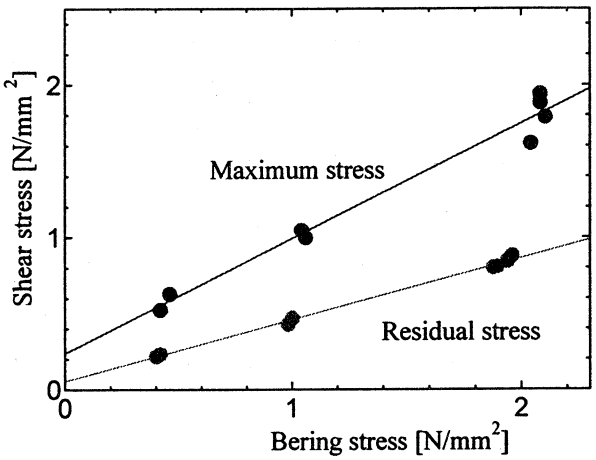

Fig. 14 Relation between shear stress and bearing stress

increase of the relative slip and then the applied load tends to approach some constant residual load. The maximum load and the residual load also increase with the magnitude of the bearing stress.

(2) Shear stress-bearing stress relation

The maximum shear stress, the relative slip at the maximum load, the residual shear stress and the relative slip at the evaluated residual load according to the relations between the load and the relative slip as shown in **Fig. 13** are summarized in **Table 3**. The residual load is defined as the load at 7.5mm slip. It can be clear from **Fig. 13** and **Table 3** that the relative slip according to the maximum load is almost less than 0.25mm in the test with the natural bond.

Fig. 14 shows the relation between the bearing stress and the maximum shear stress or the residual shear stress. The maximum shear stress or the residual shear stress is calculated from the maximum load or the residual load normalized by the contact area. The ordinate shows the shear stress and the abscissa shows the bearing stress. The regression lines are also indicated in the figure. It can be confirmed from the figure that the relation between the bearing stress and the maximum shear stress or the residual shear stress is almost linear. The slope of the regression line of the relation between the bearing stress and the maximum stress

or the residual shear stress is 0.755 or 0.405. Moreover, the ordinate intercept of the regression line between the bearing stress and the maximum shear stress or the residual shear stress is about 0.238N/mm^2 or 0.055 N/mm^2. The ordinate intercept of the relation between the bearing stress and the maximum shear stress or the residual shear stress may correspond to the bond between steel and concrete without bearing stress. This implies that some bond between steel and concrete under no bearing stress can be expected, if the shear stress does not reach the maximum shear stress. However, there is no bond between steel and concrete under no bearing stress, when the shear stress goes beyond the maximum shear stress and reaches the residual shear stress.

5. Conclusions

Nowadays, various types of steel-concrete hybrid members are employed for the bridge structures. In these structures, it is important to ensure the required stress transmission between the steel member and the concrete one. Then, some researches works associated with stress transmission behavior between steel and concrete in the steel-concrete hybrid structures are introduced in this paper.

First, the static strength and fatigue strength of the stud under the alternating load condition as well as the pulsating load condition is investigated by employing the devised push-pull test specimen. As a result, it can be seen that there is some difference between the static strength of the stud under the pulsating and alternating load conditions. However, the fatigue strength of the stud under the alternating load condition is not different from the one under the pulsating load condition. The relation between the shear force and the relative slip is useful for analyzing the responses of the stud in the hybrid structure under the earthquake motion.

Second, the strain behavior of the stud base is investigated by employing the pipe stud with the inside strain gages near the base in order to observe the strain behavior at the base of the stud shank. As a result, it can be seen that the strain behavior near the base of the stud can successfully observed through the push-pull

test. This result is also useful for checking the numerical result.

Finally, the bonding behavior between steel and concrete is investigated by employing the small scale push-out test specimen under the constant bearing stress. As a result, it can be seen that the relation between the bearing stress and the maximum shear stress or the residual shear stress is almost linear.

REFERENCES

1) Hanswille, G. : Cracking of concrete mechanical models of the design rules in EUROCODE4, Conf. Report, Composite Construction in Steel and Concrete III, ASCE, pp.420-433, 1997.
2) Committee on Hybrid Structures, JSCE : Guidelines for Performance Verification of Steel-Concrete Hybrid Structures, JSCE, 2006(in Japanese).
3) JSSC : Jssc Standard on Push-out Test for Headed Stud, JSSC Technical Report, No.35, 1996(in Japanese).
4) Gattesco, N., Giuriani, E. and Gubana, A. : Low-cycle fatigue test on stud shear connectors. Journal of Structural Engineering, ASCE, Vol.123, No.2, pp.145-150, 1997.
5) Nakajima, A., Saiki, I., Kokai, M., Doi, K., Takabayashi, Y. and Ooe, H. : Cyclic shear force-slip behavior of studs under alternating and pulsating load condition. Engineering Structures, 25(5), Elsevier Science Ltd., pp.537-45, 2003.
6) Nakajima, A., Miah, M.K., Kadogaki, T., Saiki, I. and Ooe, H. : Experimental evaluation of strain behavior of stud shear connector through shear transmission. Proc. of 5th Japanese-German Joint Symposium on Steel and Composite Bridges, pp.481-92, 2003.
7) Sonoda, K., Kitoh, H. and Horikawa, T. : Shear bond characteristics embossed steel plate with or without stud connections under a constant lateral pressure, Proceedings of the 4th ASCCS International Conference on Steel-concrete composite structures, Kosice, Slovakia, pp.307-310, 1994.
8) Nakajima, A., Nishimura, M., Saiki, I. and Ooe, H. : Interface bonding behavior between steel and concrete under bearing force, The First International Conference on Advances in Experimental Structural Engineering, Nagoya, Japan, Vol.1, pp.67-73, 2005.

TOWARD HYBRID BRIDGE DECK: AN INNOVATIVE FRP-CONCRETE COMPOSITE DECK

Byung-Suk Kim, Jeong-Rae Cho, Sung Yong Park, and Keunhee Cho
Korea Institute of Construction Technology, Korea

Abstract

FRP-concrete composite deck is an innovative structural system, which combines the advantages of both concrete decks and FRP decks and, therefore, exhibits improved durability and serviceability. The Korea Institute of Construction Technology launched a research program for developing a new type of FRP-concrete composite deck as a part of the comprehensive research program "Bridge 200" extending from 2002 to 2006. This paper gives a summary of the developed FRP-concrete composite deck including 5-year research results, presents a brief overview of the development history of the FRP-concrete composite bridge deck system, and discusses its design concepts including details of section, load resistance mechanism, design criteria, and composite effects between deck and girder. This paper also enumerates the selected research results including interfacial behavior between FRP module and concrete, details of deck-to-girder connection, static and fatigue performance of the full-scaled deck system. Finally, future work and prospects are addressed.

1. Introduction

As the most adopted bridge deck, reinforced concrete decks are requiring frequent repair, strengthening or replacement due to the loss of durability provoked by the deterioration of concrete and corrosion of steel rebar. Moreover, their excessive weight compared to the resulting strength is representing a critical constraint during the design of the girder and substructure. Recently, researches are actively conducted on FRP decks as a solution to replace reinforced concrete decks, and are seeing larger applications on field. However, despite of the advantages offered by FRP decks owing to material characteristics that are high durability, lightweight and accelerated construction, the extremely low stiffness compared to the developed strength makes the deflection the governing design factor. In addition, the exorbitant initial construction cost of FRP decks due to the high-price of FRP materials and the very high probability of local buckling at sections directly subjected to wheel loads represent the largest obstacles impeding their applicability. FRP-concrete composite decks have been conceived to achieve more efficient bridge deck system by supplementing mutually the merits and demerits

exhibited by reinforced concrete deck and FRP deck that is, the underlying FRP plays the role of formwork during casting of concrete, and then, plays the role of main member combined with concrete after curing (see Figure 1). This system takes thus optimal advantages of the materials.

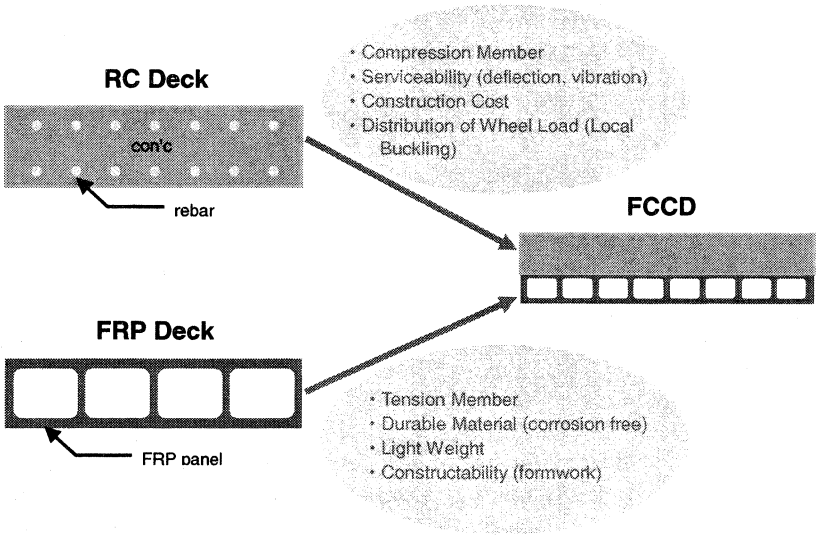

Figure 1: What is FCCD?

Recently, bridges with FRP-concrete composite decks have been actually constructed in USA and Japan applying to these concepts. The Matsukubo Bridge in Japan has been built using I-shaped FRP panel for the deck as shown in Figure 2(a). The FRP panels were used as formworks as well as complementary tensile members, and the concrete was reinforced by steel rebar. On the other hand, the Waupun Bridge in USA exploited hollowed rectangular FRP sections as formwork and major tensile member, and presented a deck reinforced by FRP grid without steel rebar, as illustrated in Figure 2(b). Compared with Figure 1(a), a hollowed zone was installed at the bottom of the deck, which realized significant alleviation of the deck's weight. The merits of the Waupun Bridge can be found in the facts that FRP panels were used as main tensile members and that corrosion problem is completely avoided by the introduction of FRP grid. Meanwhile, the Korea Institute of Construction Technology launched a research program for developing a new type of FRP-concrete composite deck independently as a part of the comprehensive research program "Bridge 200" extending from 2002 to 2006. The deck system has more simple sectional shape and has been evolved consecutively for overcoming its shortcomings revealed in various tests(see Figure 2(c)). This paper gives a summary of the developed FRP-concrete composite deck including 5-year research results, presents a brief overview of the development history of the FRP-concrete composite bridge deck system, and discusses its design concepts including details of section, load resistance mechanism, design criteria, and composite effects between deck

and girder. This paper also enumerates the selected research results including interfacial behavior between FRP module and concrete, details of deck-to-girder connection, static and fatigue performance of the full-scaled deck system. Finally, future work and prospects are addressed.

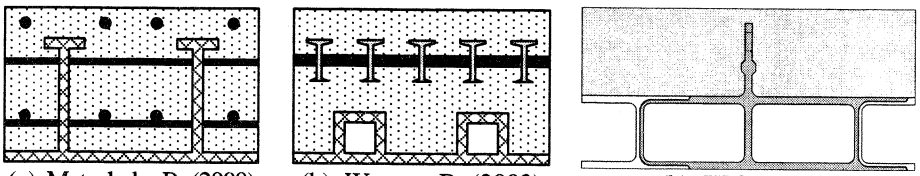

(a) Matsukubo Br.(2000) (b) Waupun Br.(2003) (b) KICT(2005)

Figure 2: Typical FCCD sections

2. Development History

Figure 3 depicts the evolution of the sectional shapes of the FRP module constituting the FRP-concrete composite deck developed by KICT. The original module of 2002 and 2003 shown in Figure 3(a) was fabricated by casting concrete above the FRP module. The module was made by attaching successively the FRP tubes that have been produced by pultrusion and, then, by bonding the FRP plates manufactured by hand lay-up at the upper and bottom of the tubes so as to create a sandwich-shape (In 2002, upper plate was not introduced). The bond strength was strengthened by applying coarse sand coating at the FRP-concrete interface. The utilized quantity of FRP converted into deck thickness reached about 38.75mm. Tests results revealed that failure initiated at the connection between the FRP tubes and between the FRP plates and tubes. According to the fact that the modules were completed through assemblage of all the members by block-laying, the failure at the interface between the FRP members was an undesirable failure mode. [1,2] Therefore, the fabrication of the FRP section of the deck as a unique module arose as a solution to overcome this problem. The developed model illustrated in Figure 3(b) was obtained by pultrusion of a unique module. The total height of the module, the spacing of the webs and the thicknesses of the flanges and webs were determined considering synthetically the fabrication thickness allowing quality control and an optimal process resulting from structural analysis. Coarse sand coating was also applied at the interface between FRP and concrete. The connection between the FRP modules was realized by applying epoxy on the male-female socket-shapes given to the extremities of the modules. At the same time, mechanical connection between FRP and concrete was also examined as an auxilary connection method for the soft-landing to the market, although we believe that coarse sand coating is enough for the connection between FRP and concrete. For the mechanical connection, it is devised that shear connecting plates with H-shape is bonded to FRP module with epxoy. Some direct shear tests were conducted regard to the height and bonding surface chosen as test variables. Tests revealed that the effects of the so-fabricated shear connecting plates were largely below the expectations. The shear connecting plates fabricated separately and bonded to the FRP modules were seen to fail at first at the bond interface, which disabled the connecting plates to fulfill

their functions.[3]
The model 2005 depicted in Figure 3(c) was conceived to overcome this shortcoming by fabricating the shear connecting plates and FRP module as a monolithic section. The thickness of the flanges was adjusted by reflecting the experimental results obtained from the previous model. The utilized quantity of FRP including the shear connecting plates reached 28.67mm, which represents a reduction of approximately 26% compared to the model 2003. Since the surface applied with epoxy for the assembling is reduced by about 73%, the proposed model achieves remarkable improvements in terms of economic efficiency and constructability. Diversified tests were then conducted to evaluate the structural performances of this innovative model improved throughout such development process.[4]
Even if the model 2005 exhibited remarkable performances under static and wheel load rolling tests, the small thickness of the concrete cover above the shear connecting plate provoked the initiation of cracks at the shear connecting plate due to drying shrinkage. Accordingly, the model 2006 decreased the height of the shear connecting plate as illustrated in Figure 3(d) and improved the quality control as well as the constructability. The execution of wheel load rolling tests and trial construction are scheduled this year for this new model.

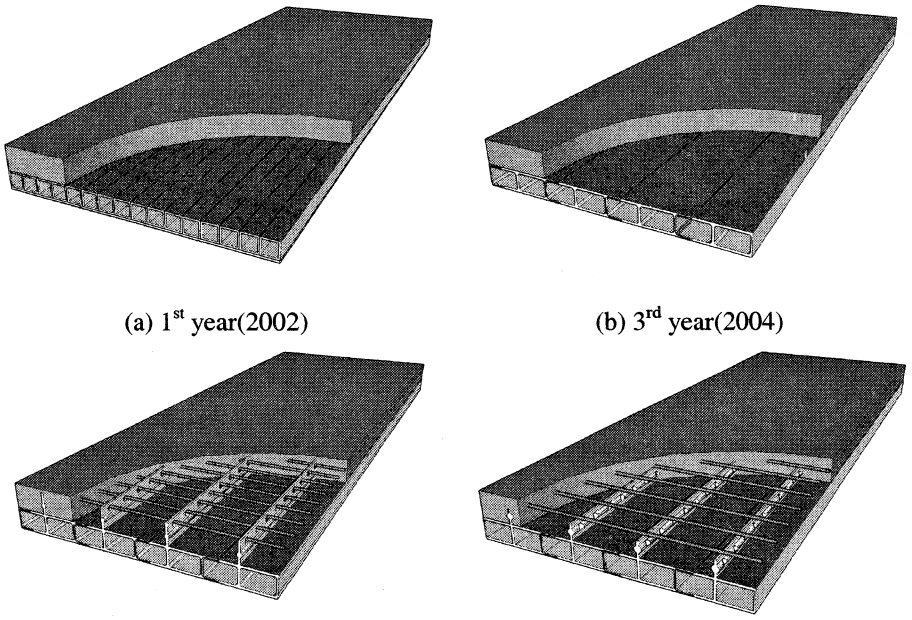

(a) 1st year(2002) (b) 3rd year(2004)

(c) 4th year(2005) (d) 5th year(2006)

Figure 3: Evolution of section shape

3. Design Concepts

3.1 Details of Section

A prerequisite of extreme importance in the development of FRP-concrete composite decks is the solidity of the composition between FRP and concrete. The techniques applied to achieve such composition are the chemical coupling using materials like sand coating and the mechanical coupling using shear connecting plate. Coarse sand coating is a method which bonds the aggregates with diameter of 4~7mm to the FRP surface by means of epoxy. In steel deck system, this method is usually applied in order to prevent sliding and infiltration of water between concrete and asphalt. Shear connecting plate is a member connected perpendicularly to the upper face of the FRP member, which plays the role of shear key.

This study opted for a solution combining both coarse sand coating and shear connecting plate in order to realize the connection of concrete and FRP, as depicted in Figure 4. Particularly, a protrusion has been left at the foot of the shear connecting plate to prevent the vertical separation between FRP and concrete, and a hole has been reserved in the protrusion so as to allow concrete to develop pullout resistance. Moreover, the shear connecting plate is also used for the fixation of the reinforcing bars as illustrated in the figure.

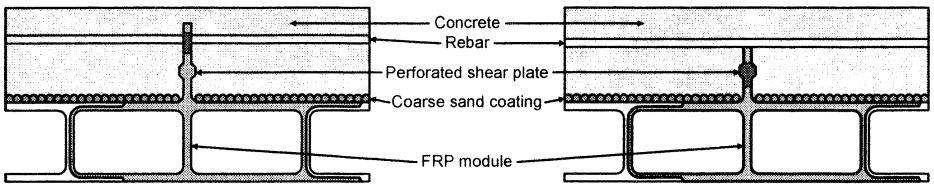

(a) Model with rebar passing through the hole

(b) Model with rebar supported by the shear connecting plate

Figure 4: Details of section

3.2 Load Resistance Mechanism

The presence of the interface between the two main materials of FRP-concrete composite decks produces unavoidably a definite slip. However, the insignificance of this slip allows the assumption of a perfect composition[5]. In addition, even if the difference in the stiffness and sectional shapes of concrete and FRP discards the possibility to satisfy a strict linearity in the strain distribution inside the section, it has been verified experimentally that the strain distribution is quasi-linear[4]. Accordingly, assumption is done for a linear strain distribution in the FRP-concrete composite deck section as shown in Figure 5.

In the positive moment zones between the girders, concrete at the top is generally resisting to compression while FRP sustains traction at the bottom. On the other hand, in the negative moment zones above the girders, FRP at the bottom is playing the role of main compressive member while rebar is fulfilling the role of main tensile member rather than concrete. The sectional resisting moment can be derived easily as for RC

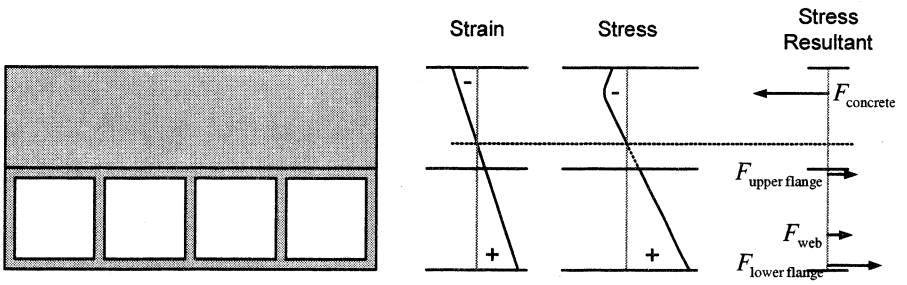

(a) Positive moment zones

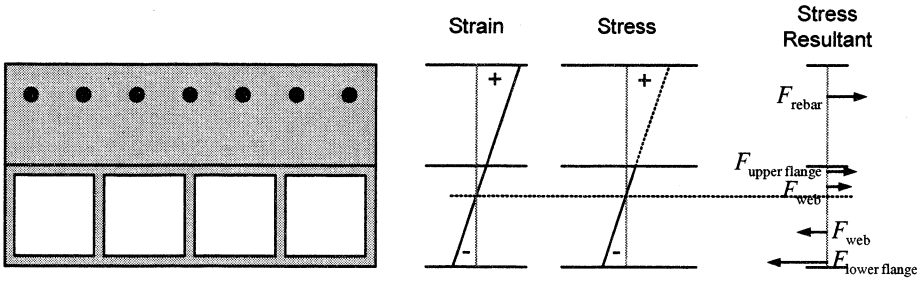

(b) Negative moment zones

Figure 5: Load resistance mechanism

deck using the assumed strain distribution, stress-strain relationship and the equilibrium of forces.

3.3 Design Criteria

The FRP-concrete composite deck to be developed in this study is similar to a steel-free deck regard to its structural type and load resistance mechanism. However, the adoption of the design concept illustrated in Figure 6 enables to achieve significant increase of the stability of the deck constituted by two brittle materials. At the initial loading stage, FRP and concrete exhibit perfect composite behavior and, finally, failure starts with concrete due to fatigue. Then, the section modifies into a structure resisting through FRP only. Nevertheless, design has been conceived to secure a safety margin exceeding 2 under service load even with FRP only, which enables to prevent brittle fracture. Accordingly, even if the FRP-concrete composite deck to be developed in this study is composed by two brittle materials, the proposed innovative deck is increasing safety in that signs announcing failure can be detected in advance, which secure sufficient time to prepare and establish preventive measures.

3.4 Composite Effects between Deck and Girder

The composite effects of steel girders have been investigated for RC decks, FRP decks and FRP-concrete composite decks. The considered sections are illustrated in Figure 7.

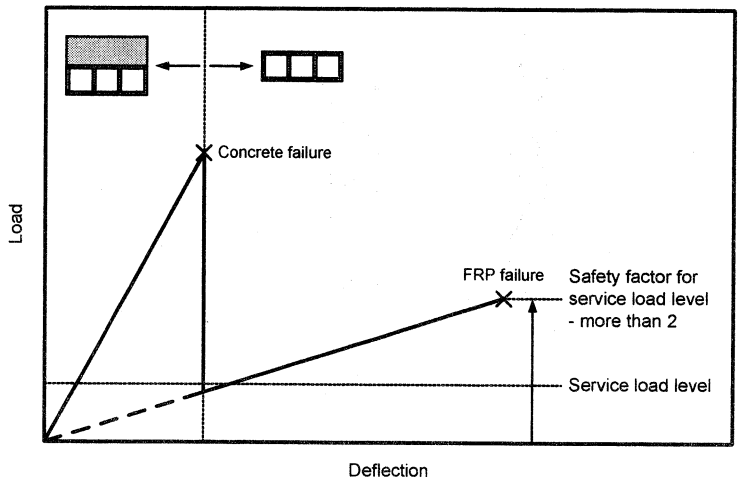

Figure 6: Design criteria

Figure 8 expresses graphically the effects of the composition and non-composition on the increase of strength. The sectional strength induced by the composition of RC decks, FRP decks and FRP-concrete composite decks reaches respectively 221%, 120% and 198% regard to the strength of the sole girder. Especially, during the composition of the FRP-concrete composite deck, the sectional strength reaches 90% of that of RC deck, which represents a remarkable strength-increasing effect. Consequently, a composite design appears to be advantageous in terms of fatigue of the girders or serviceability like the deflection.

The volumetric weights of each of the decks have been compared as shown in Table 1. For the comparison, the minimum deck thickness of 22cm with respect to the current Korean Bridge Design Code was applied for the heights of the RC deck and FRP-concrete composite deck. The FRP deck was decided with reference to the actually

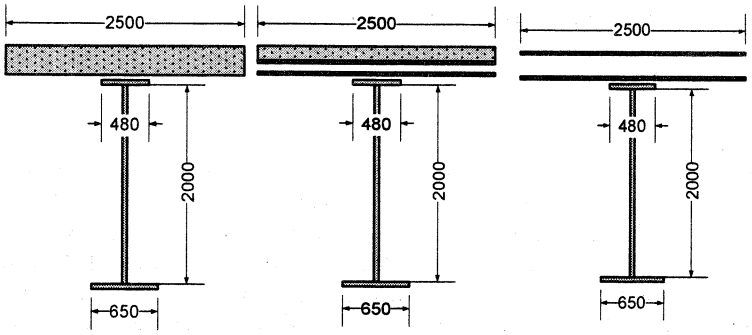

Figure 7: Cross-sections of steel girders and decks

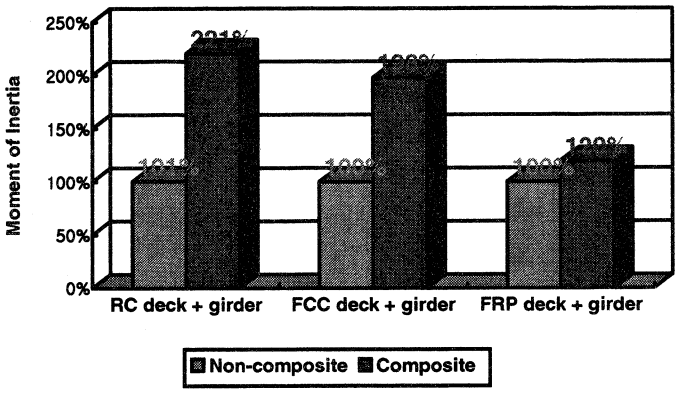

Figure 8: Comparison of composite effects according to the types of deck

Table 1: Comparisons of volumetric weight according to the types of deck

Deck type	Height	Volumetric weight	Weight ratio
RC deck	22cm	0.55 tonf/m^2	100%
FRP deck	20cm	0.09 tonf/m^2	16%
FRP-concrete composite deck	22cm	0.35 tonf/m^2	64%

※ The weight ratio corresponds to the ratio to RC deck

constructed bridge. Comparison results revealed the volumetric weights of the FRP-concrete composite deck and FRP deck reach approximately 64% and 16% of the one of the concrete deck, respectively, which demonstrates that the FRP-concrete composite deck gives significant reducing effect on the dead load compared to previous concrete decks. Even if lighter than the RC deck with a weight ratio of about 64%, the FRP-concrete composite deck exhibits a composite effect reaching 90% of steel girder, which shows that the composite effect of steel girder is extremely large.[5]

4. Behavior of FRP-Concrete Interface

4.1 Sand Coating

The characteristics of the FRP-concrete interface have been studied at the initial stage of the present R&D program. Direct shear tests were conducted on the specimen illustrated in Figure 9(a). The bond-slip model for coarse sand coating shown in Figure 9(b) was derived by minimizing the difference between the experimental strain of FRP and the theoretical strain obtained from a bond-slip model based on fracture mechanics. The optimized bond-slip model gave bond strength of 1.43MPa and fracture energy of 700N/m.[6]

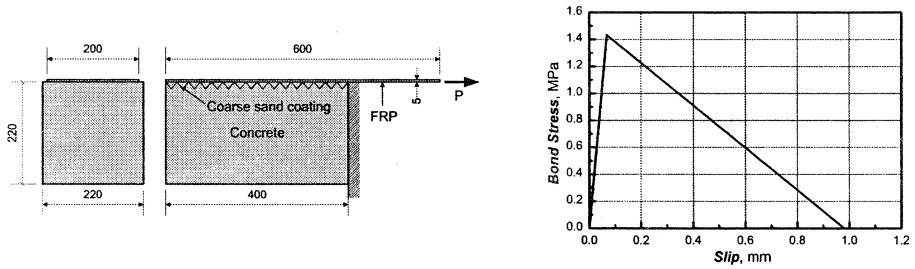

(a) Shape of the bond test prototype (b) Optimized bond-slip model

Figure 9: Direct shear test for coarse sand coating at FRP-concrete interface

4.2 Shear Performance Evaluation Test

As mentioned in Section 2 and 3.1, coarse sand coating and shear connecting plates were applied simultaneously to secure composite effect between FRP and concrete since 2005. Shear tests were conducted on 2 sets of 2 specimens to evaluate the transverse (SH-1, SH-2) and longitudinal (SH-3, SH-4) shear performances of the FRP-concrete interface as illustrated in Figure 10. FRP rebars were disposed to prevent the fracture of the concrete blocks and the FRP-concrete interface was set with width of 300mm and height of 600mm.

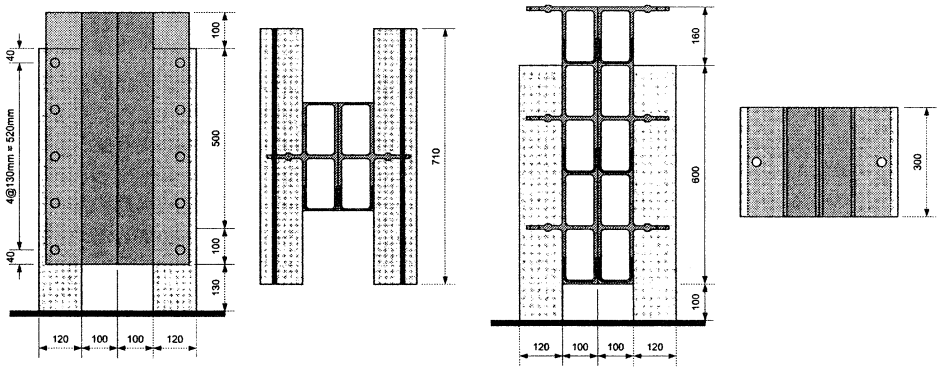

(a) Transverse direction (SH-1, SH-2) (b) Longitudinal direction (SH-3, SH-4)

Figure 10: Shape and dimensions of the shear performance evaluation test specimens

Tests revealed that the transverse specimens (in the direction of the connecting plate length) failed at an average failure load of 1,792kN at the interface between FRP and concrete, while the longitudinal specimens (direction transverse to the connecting plate) failed at an average failure load of 1,866kN also at the interface between FRP and concrete as shown in Figure 12. The bond strengths obtained for the case where only coarse sand coating is applied using the bond-slip model of coarse sand coating (Figure 9(b)) were determined to be 401kN in the transverse direction and 420kN in the

longitudinal direction. A simple comparison of the experimental results based on these analytical values shows that the bond strength at the FRP-concrete interface increased by about 4.5 times through the addition of the shear connecting plates compared to the use of coarse sand coating only. More precise comparison will be performed this year after direct shear tests on specimens using only coarse sand coating. However, the actual results are already demonstrating that the installation of shear connecting plates is achieving significant improvement of the bond performance at the interface. [7]

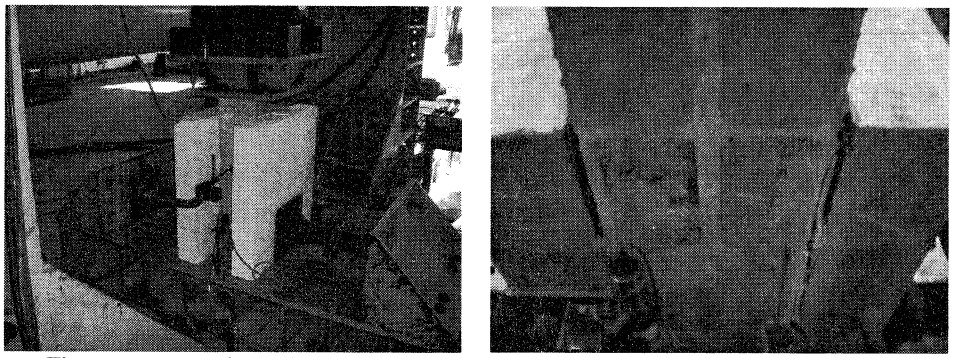

Figure 11: Overview of shear performance evaluation test and failure of interface

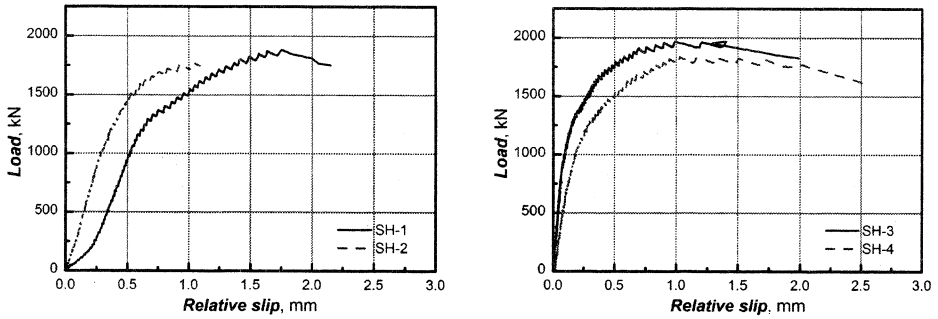

(a) Transverse direction (SH-1, SH-2) (b) Longitudinal direction (SH-3, SH-4)

Figure 12: Direct shear test: load-displacement curves

5. Details of Deck-to-Girder Connection

The connection details of the developed FRP-concrete composite deck with the girder have been proposed with reference to the connection used in precast decks. As shown in Figure 13, shear pockets are shaped in the FRP module to receive the shear connectors. Once the shear connectors are installed, non-shrinkage mortar is poured. Then, welding studs are disposed over the girder in the case of steel girders, or U-shaped stirrups in the case of concrete girders.

In order to examine the proposed girder connection, shear performance evaluation tests

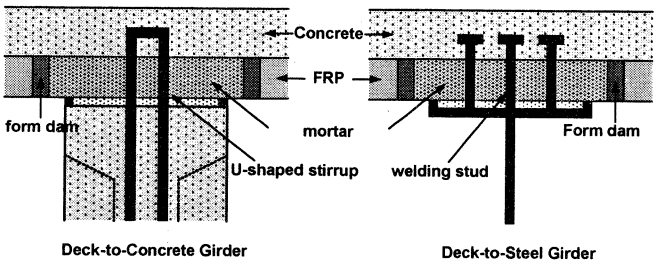

Figure 13: Details of deck-to-girder connection

were conducted on two sets of two steel girder and concrete girder specimens manufactured with shapes corresponding to standard pull-out specimens prescribed by Eurocode 4(see Figure 14). The performance evaluation tests revealed that the deformation concentrated at the connection between the deck and girder so as to provoke failure(see Figure 15 and 16). The resisting strength exceeded the strength required in the Korean Bridge Design Code (2005) by 1.83 times, which verified that sufficient safety is secured(see Table 2).[5]

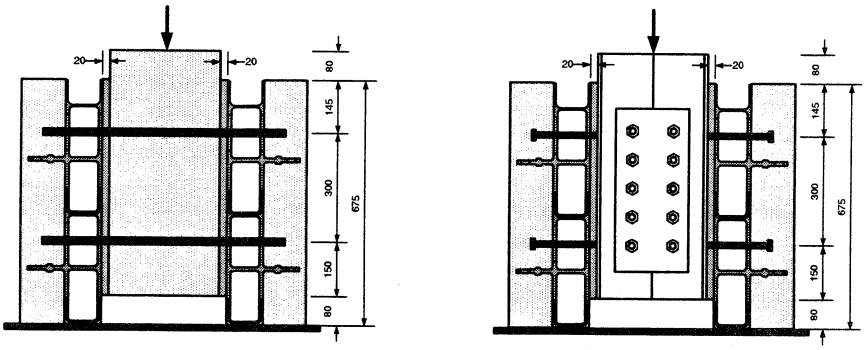

(a) Transverse direction (SH-1, SH-2) (b) Longitudinal direction (SH-3, SH-4)

Figure 14: Shape and test layout of the deck-girder composite specimens

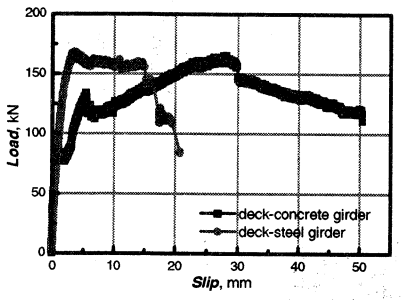

Figure 15: Load-displacement curve

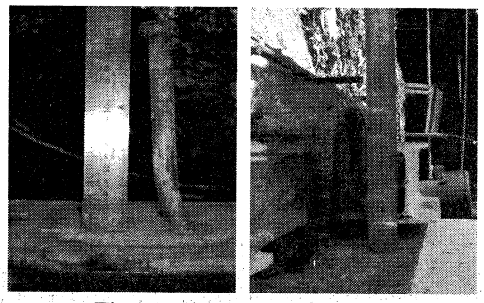

Figure 16: Shapes of failure

Table 2: Comparisions between resisting strength and desgin strength

Type	Resisting strength (kN)	design strength (kN)	(Resisting strength) / (design strength)
Stirrup (Concrete Girder)	88.0	48.2	1.83
Stud (Steel Girder)	168.2	92	1.83

6. Structural Performance

The composite deck with a span of 2.5m illustrated in Figure 17 has been adopted for the static loading test and moving wheel road test. Holes of 25mm diameter were perforated with spacing of 150mm in the shear connecting plates at a height of 75mm from the top flange of the FRP modules to the center of the holes. In addition, FRP reinforcements were introduced longitudinally through these holes with a reinforcing ratio of 0.436%.[2,3]

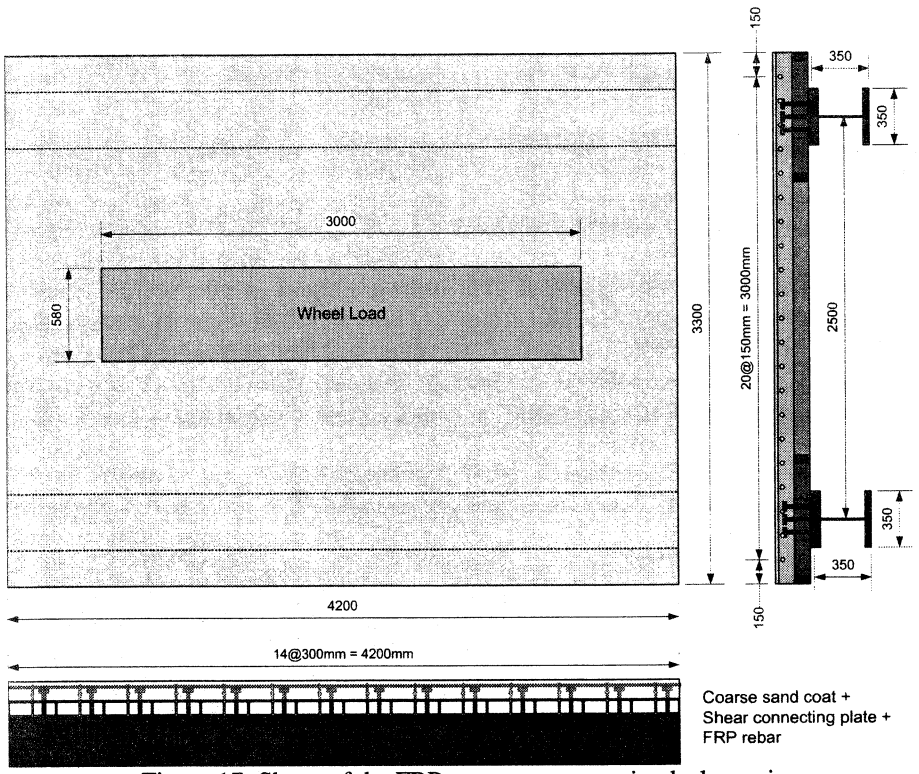

Figure 17: Shape of the FRP-concrete composite deck specimen

6.1 Static Performance

A surface load simulating the size of the wheel was applied on the center of the deck by load control at a speed of 0.1kN/sec up to 124.8kN. After that value, load was applied by displacement control at a speed of 0.01mm/sec until failure. The bottom flange of the girder of the specimen was fixed to the support block by means of bolts so as to simulate realistically the restraint effects due to the cross-beam in actual bridges. Figure 18 shows an overview of the static loading test.

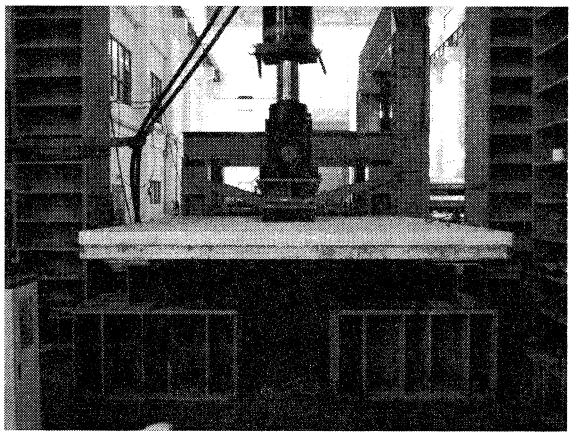

Figure 18: Overview of static loading test of the deck specimen

Figure 19 plots the load-displacement relationships observed for the whole testing process. Crack occurred in the negative moment zone above one of the girder at 530kN and developed also in the negative moment zone of the other girder at 580kN. Thereafter, load continued to increase up to 971kN at which punching failure occurred under deflection of 17.7mm.

Gauges were installed inside the deck to observe the bonding failure occurring at the interface between FRP and concrete. The first bonding failure happened at location (A) at mid-span under load of 410kN corresponding to a deflection of 5.8mm. Then, bonding failure occurred at location (B) located at a transversal distance of 450mm far away from the center under load of 938kN and deflection of 16.7mm. After punching failure, a deflection of 22.7mm under loading of 831kN was observed at point (C) located at a distance of 900mm far away from the center. After occurrence of punching failure, the resistance to load continuously decreased according to the increase of deflection to finally result in the failure of the connection between FRP modules at the loading points.

The deflection developed under loading of 124.8kN, which corresponds to DB-24 rear wheel load considering impact (maximum design wheel load in Korea), was 1.51mm. Assuming a limit criterion of L/800 (L: span length) for the deflection of the deck, that is 3.125mm, the deck is seen to satisfy sufficiently the design criterion. Moreover, no damage was observed in the deck specimen until that point of time. Considering that the failure load is 971kN, a safety factor of 7.8 is secured.[4]

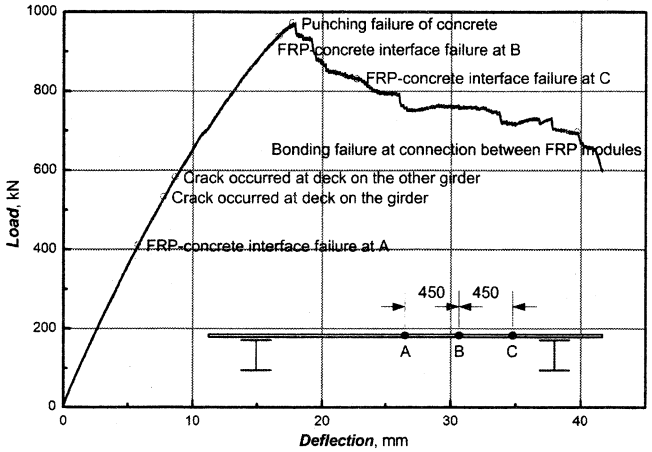

Figure 19: Load-displacement relationship

6.2 Fatigue Performance

To test fatigue performance, moving wheel road test[8] was performed as shown Figure 20. Considering the safety factor and impact to the 96knN of the DB-24 rear wheel load, the level of loading was decided to be 149.76kN as expressed in the following equation.

$$P = 96\text{kN}\,(\text{DB - 24 rear wheel load}) \times 1.3(\text{Impact coef.}) \times 1.2(\text{Safety factor}) = 149.76\text{kN} \quad (1)$$

Static loading test was performed every 50,000 cycles in order to evaluate the degree of fatigue-induced damage. The static test applied loading up to 124.8kN so as to assess fatigue-induced damage under service load.

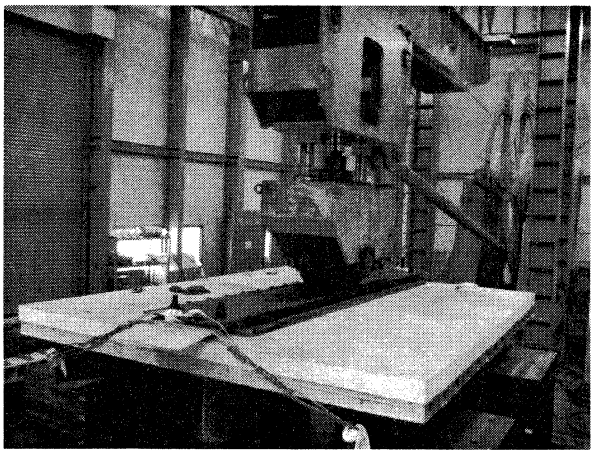
Figure 20: Overview of moving wheel road test

The deflection, δ_i, obtained through the wheel rolling test can be divided into $\delta_{f,i}$ expressing the deflection due to the accumulation of damage under repeated wheel loading and $\delta_{s,i}$ standing for the deflection occurring under static loading.

$$\delta_i = \delta_{f,i} + \delta_{s,i} \tag{2}$$

where $\delta_{s,i}$ is closely related to the resistance of the deck to loading, and $\delta_{f,i}$ corresponds to the residual deformation of the deck. However, no study has been performed to date to determine which of these two components is the most dominant for the fatigue performance of the deck.

Figure 21 illustrates the fatigue deflection developed under wheel loading cycles. It can be observed that the total deflection, δ_i, is increasing with stiffer slope than the residual deflection, $\delta_{f,i}$, while the difference of slopes is not large. Therefore, the static deflection, $\delta_{s,i}$, is slightly increasing compared to the total deflection and the residual deflection. Consequently, the resistance of the deck to loading can be seen to be maintained without serious damage until 2,000,000 loading cycles. [9]

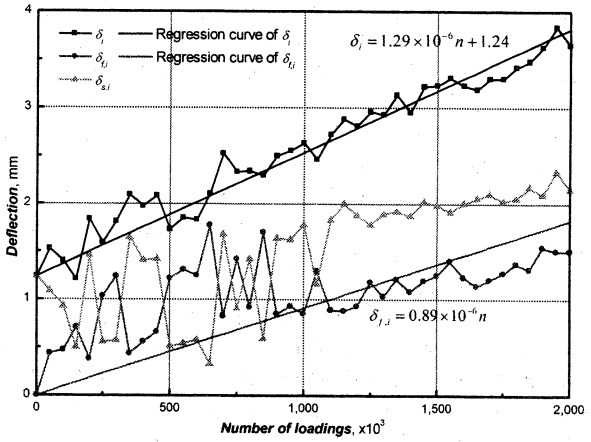

Figure 21: Increase of deflection due to wheel loading

7. Concluding Remarks

The development history of FRP-concrete composite bridge decks implemented by the Korea Institute of Construction Technology has been overviewed and selective results have been discussed. Currently, a trial construction and field tests are planned on a temporary highway bridge. This year, wheel load rolling tests are under course for the improved deck shape. Research results to date demonstrated that sufficient safety is secured for the application of the developed deck on field. The problem resides in the inherent expensiveness of FRP material, which results in initial construction cost relatively higher than former RC decks. Analyses considering lifecycle cost shall be

performed from which outputs will be used to persuade the orderer. Under such conditions, it is believed that the application of the developed deck will be forwarded. Especially, need is to promote applications in coastal and marine areas where bridges are exposed to corrosive environment.

8. Acknowledgements

This research is funded by the project for the development of long-life deck systems for bridges, an in-house program of the Korea Institute of Construction Technology.

9. References

1. Korea Institute of Construction Technolgy, Development of Long-Life Deck Systems for Bridges (I), 1st Annual Report, 2002 12. (in Korean)
2. Korea Institute of Construction Technolgy, Development of Long-Life Deck Systems for Bridges (I), 2nd Annual Report, 2003. 12. (in Korean)
3. Korea Institute of Construction Technolgy, Development of Long-Life Deck Systems for Bridges – Steel Free Deck, 3rd Annual Report, 2004. 12. (in Korean)
4. Korea Institute of Construction Technolgy, Development of Long-Life Deck Systems for Bridges – Steel Free Deck, 4th Annual Report, 2005. 12. (in Korean)
5. Cho, K., Cho, J.R., Kim, S.T., Chin, W.J. and Kim, B.S. "Analysis of Composite Behavior between FRP-Concrete Composite Deck and Girder" Annual Spring Conference of Korea Cocrete Institute, 2005.5. 379-382. (in Korean)
6. Cho, K., Cho, J.R., Chin, W.J. and Kim, B.S., "Bond-slip model for coarse sand coated interface between FRP and concrete from optimization technique", *Computers & Structures*, Vol. 84, pp. 439-449, 2006. 1.
7. Park, S.Y., Cho, K., Cho, J.R., Kim, S.T. and Kim, B.S. "Updated FRP-Concrete Composite Bridge Deck System", The Tenth East Asia-Pacific Conference on Structural Engineering and Construction (EASEC-10), 2006.8., 567-572
8. Kim, Y.J., Cho, C.B. and Kim, B.S., A Study on Development of Wheel Load Testing Equipment, Annual Conference of Korean Society of Civil Engineers, Korea, 2003, 529-534.
9. Cho, K., Park S. Y., Cho, J.R., Kim, S.T. and Kim, B.S. "Evaluation of Wheel Load Fatigue Performance of FRP-Concrete Composite Deck", The Tenth East Asia-Pacific Conference on Structural Engineering and Construction (EASEC-10), 2006.8., 261-266

Hybrid Bridges on Expressway in Japan

Takeshi OHSHIRO
Central Nippon Expressway Co. Ltd., Japan

Abstract
The steel-concrete hybrid bridges, for example the prestressed concrete box girder with corrugated steel web, the hybrid arch bridge and the composite truss bridge, have been adopted generally on expressway in Japan. This paper is the introduction of major hybrid bridges on expressway in Japan.

1. Introduction

The technology of the prestressed concrete bridge in Japan has been developed greatly in the latest ten years. Especially, the steel-concrete hybrid bridges have been adopted generally on expressway in Japan. For example, the prestressed concrete box girder with corrugated steel web has been adopted on expressway more than 70 cases, and it is a general bridge type now. This paper is the introduction of major hybrid bridges on expressway in Japan.

2. Extradosed Bridge with Corrugated Steel Web –Himi Yume Bridge–

2.1 Himi Yume Bridge

The Himi Yume Bridge is newly constructed a composite extradosed bridge with corrugated steel web. This is the first application for the cable-supported bridges in the world. A variety of new technologies was used in the bridge. The bridge completed in March 2004, and opened to traffic on the Nagasaki Expressway.

2.2 Design

In the early planning stages, priority has been given to structural form, aesthetic appearance and harmony with the environment in the design of this bridge. The result is the world's first extradosed bridge with corrugated steel web. In the design of the bridge, "durability" and "lightweight" were mainly concerned. The selection of the height and the section shape of the main girders has been focused on economy, ease of construction and streamlined configuration, and it was necessary to achieve a configuration that was as slender as possible with the objective of reducing the weight of the girders, and based on aesthetic appearance as well. For this reason, the following were established as

preconditions for the design.
(1) The main girders should be a constant height.
(2) The main girder section should be a wide single box girder.
(3) The use of a composite structure for the main girder extradosed cable anchorage configuration should be studied.
(4) No internal tendons should be used.

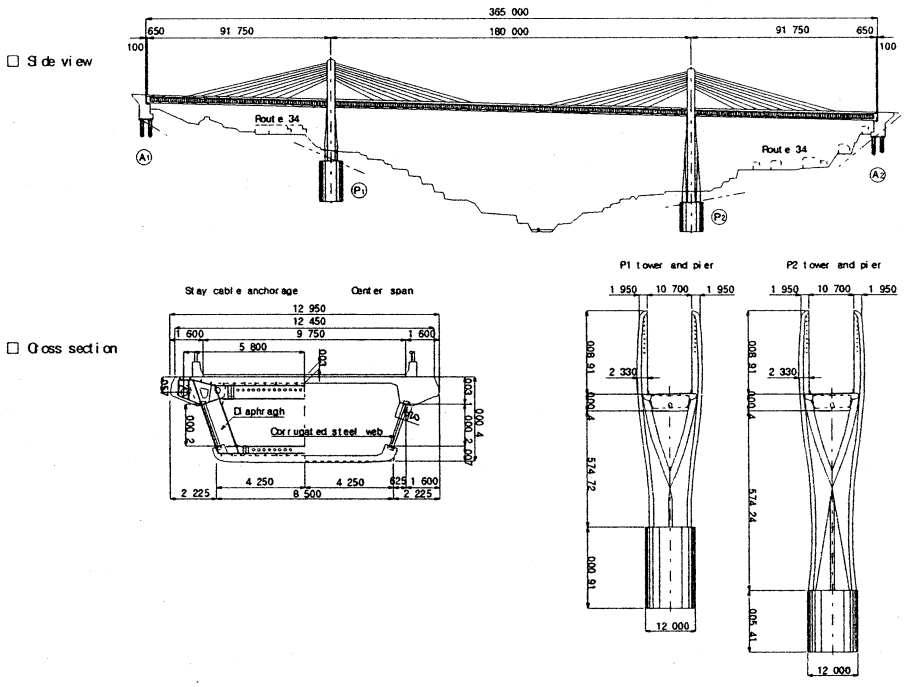

Figure 1: General view

2.3 Extradosed cable anchorage

The preconditions for determination of the extradosed cable anchorages for the main girders are that the vertical component of the extradosed cables must be transmitted efficiently to the main girders, that little additional stress should be applied to the corrugated steel web, and that the weight of the main girders themselves should be reduced. The composite diaphragm, in which both vertical and horizontal ribs were reinforced with steel members, was intended to be both more rational and more lightweight.

The corrugated steel webs were joined using single plane lap splice fillet welding.

Furthermore, the method used to join the concrete slab and corrugated steel webs was an angle dowel using flange plates. Accordingly, the corrugated steel webs and diaphragm were fused into a single unit through complete joint penetration welding on the same web surface, so the vertical component of the extradosed cables and the shear force of the main girders could be transmitted smoothly.

As the mechanism by which extradosed cable force is transmitted, the structure is one in which vertical force is transmitted from the stay cable anchorages through the concrete to the diaphragm. When this occurs, it is predicted that localized stress will be produced at the joints between the corrugated steel web and the concrete short web and near the corners of the corrugated steel plates and the diaphragm. Accordingly, the 3D FEM analysis will be conducted to determine local stress, and after the detailed structure of the joints has been finalized, the safety of this structure will be confirmed through experimentation and then the results will be reflected in the actual bridge.

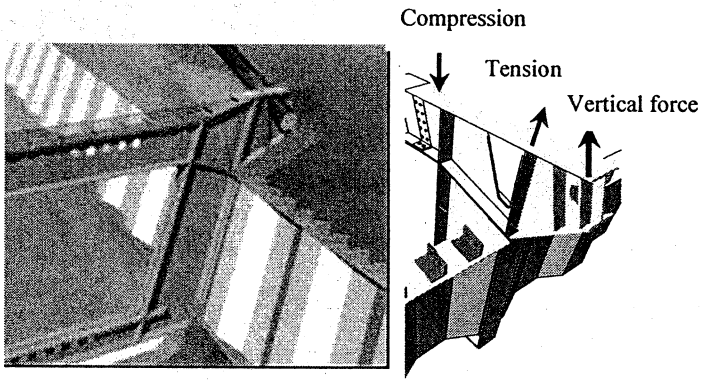

Figure 2: Bird's-eye view of extradosed cable anchorage

2.4 Construction

A major feature of this bridge is the fact that the use of an ultra-large form traveler (10000 kN.m capacity) made it possible to use a standard segment length of 6.4m, enabling the number of cantilever blocks to be reduced and shortening the work time. This form traveler was three times as large as ordinary ones, and it enabled the number of segment to be reduced by half, greatly contributing to shortening the amount of time required for the work and constituting a very economical method of construction as well.

Prefabricated cables were used as the extradosed cables in order to reduce the amount of work at the site and thereby reduce labor requirements. Furthermore, a steel shell configuration was used for the extradosed cable anchorages on the main tower. This configuration combines the superiority of factory manufacture with a reduction of the labor required for construction at the site.

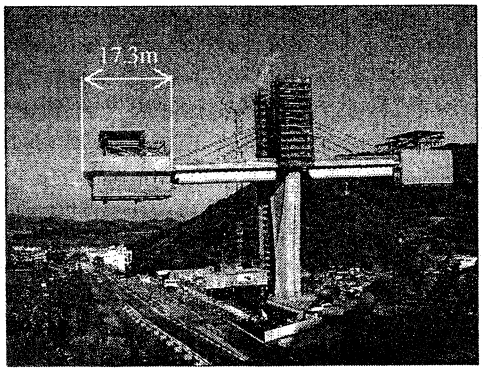

Figure 3: Erection work

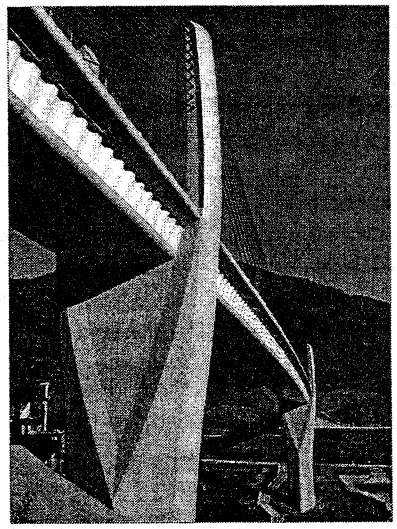

Photo 1: Himi Yume Bridge

2.5 Conclusions

The Himi Yume Bridge is the world's first bridge to combine the use of a corrugated steel web configuration with the extradosed mode whose use has developed rapidly in Japan in recent years. A variety of new trials has being implemented in the design and construction of this bridge.

In February 2002, a 1/2 scale model test and wind tunnel test were planned in order to verify and confirm the safety of the configuration.
In these new efforts, issues linked to the expanded application of extradosed bridges have been resolved, and innovative technical efforts aimed at development further have been conducted, in preparation for the completion of the bridge in 2004.

3. Prestressed Concrete Corrugated Steel Web Box Girder with Ribs and Struts

3.1 Katsurajima Viaduct

The Katsurashima Viaduct, a 216-meter-long 4-span continuous prestressed concrete box girder bridge, is located in the approximate center of the second TOMEI expressway.

The bridge was constructed in a mountainous region with very irregular terrain. Accordingly, in order to make the incremental launching method more streamlined and economical, a corrugated steel web was introduced to reduce the weight of the bridge. In addition, a new method called separated-section method that involves the use of ribs and struts was developed, and it was decided to conduct the incremental launching process with a section for which the wing slab was constructed later (hereafter "core section").

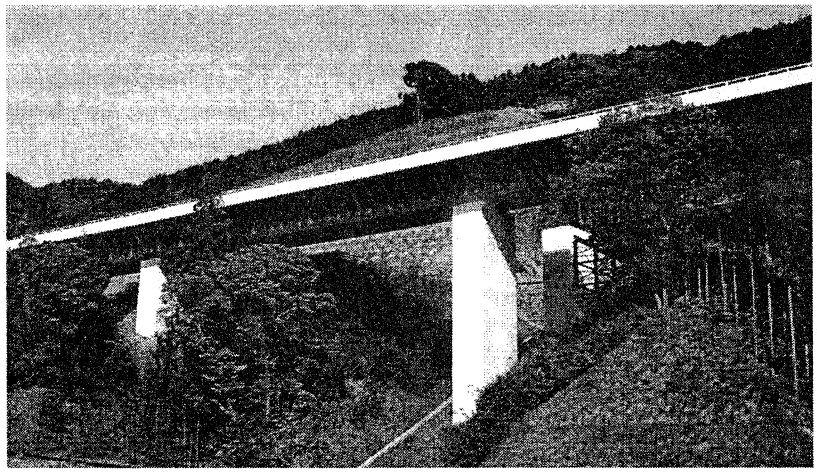

Photo 2: Katsurashima Viaduct

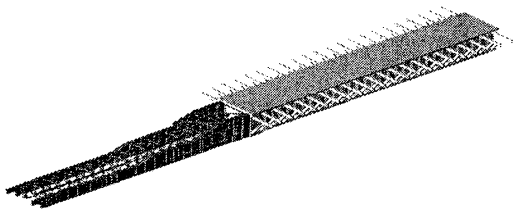

Figure 4, Photo3:
Incremental launching using the core section

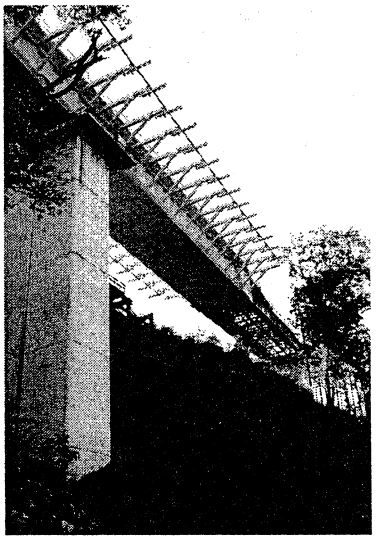

The result was the achievement of an efficient and economical bridge, using a construction method and structure without parallel anywhere in the world: a corrugated steel web box girder bridge with concrete ribs and struts, constructed by means of incremental launching using the core section.

3.2 General Description

(1) Corrugated Steel Web Box Girder Structure with Ribs and Struts

The structure is one in which the upper slab of a conventional corrugated steel web box

girder bridge is supported with ribs and struts. The use of this structure enables the wing slab to be lengthened and makes it possible for the box girder to have a narrower lower slab. Therefore, the weight of the superstructure and the pier width to be decreased.

(2) Incremental Launching by Means of Separated-Section Method

The use of ribs and struts on this bridge enabled the wing slab to be lengthened, and the use of corrugated steel for the web enabled the dead load to be reduced. As a result, the proportion of the weight of the wing slab by the total bridge weight was comparatively great (approximately 35% of the total bridge weight). Accordingly, the weight during the incremental launching process can be greatly reduced by conducting incremental launching with a core section containing no wing slab. For this reason, it was decided to construct this bridge through incremental launching, using a new method unparalleled anywhere in the world: separated-section method. The weight at the launching stage is decreased by 50% of the overall weight, which lowers the requirements for the launching nose, jacks, and other erection equipment. It also reduces the amount of prestressing strand required when the main girder is put into place.

(3) Upper Slab Comprising Prestressed Concrete Precast-Panels and Cast-in-Place Concrete

The upper slab is constructed by setting prestressed concrete precast-panels onto the ribs, and using these panels as permanent formwork for cast-in-place concrete. This method reduces formworks, supports and the amount of work required, shortening the construction period. And this reduced manpower requirements for the construction of the wing slab following the completion of the incremental launching process. PCPca-panels were placed between the ribs using a miniature crane placed on the bridge surface, and these were used as formwork for the placement of the concrete. This made form travelers unnecessary for the later stages of construction.

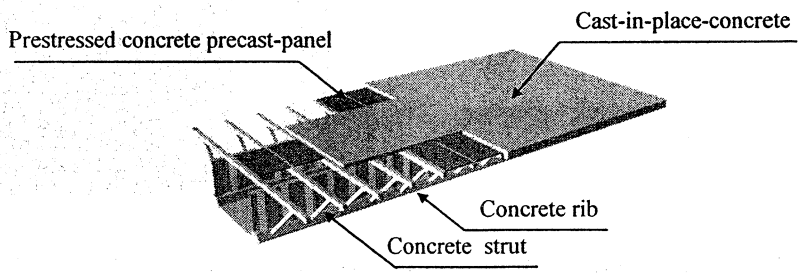

Figure 5: Construction method of upper slab

(4) Diversion of Launching Erection Cables for Use in Completed Bridge

With the conventional method of incremental launching construction using the full external tendon method, some of the cables placed in the zigzag pattern are not needed

when the bridge is completed. These cables are removed and other cables are added where an insufficiency exists. When the incremental launching method was used for construction, this had the problem of increasing the total number of prestressing cables used. Accordingly, the pattern in which the temporary cables used for erection were placed was changed to the straight up and down pattern. This enabled the tension of the prestressing cables placed on the top side to be released following the completion of the incremental launching process. Their placement was then changed for retensioning and diversion to use as tendons on completion.

3.3 Conclusions

The Katsurashima Viaduct, which has a structural form that is the world's first: a corrugated steel web box girder bridge with concrete ribs and struts was completed in May 2005. The bridge used an effective combination of ribs, struts, PCPca-panels and corrugated steel web along with cast-in-place concrete and represents a new composite structure bridge in which these elements were used effectively from construction through completion. This structure is an extremely effective method in an area of prestressed concrete bridges (those with span length 40 - 60 m) that had previously not been one of specialties. This method is expected to expand further the applicable range of prestressed concrete bridges.

4. Steel and Concrete Hybrid Arch Bridge

4.1 Fujikawa Bridge

The Fujikawa twin arch bridges form parts of the second Tomei Expressway Project, which provides a link in the "Tokaido route", a main Japanese route between Tokyo and Nagoya, running along Pacific coast. The bridges are the first steel-concrete hybrid arch bridges in Japan, which consist of reinforced concrete arch and steel girders for the superstructure.

This report describes the characteristics of the structure, design and construction of this bridge.

4.2 General Description

The bridges consist of A-line bound for Tokyo and B-line bound for Nagoya. The deck of A-line is 365m long with 2×28.25m spans+10×28.0m spans+28.5m span, another B-line is 381m long with 2×26.5m spans+10×27.7m spans+2×25.5m spans. The superstructure is a twin steel girder carrying prestressed concrete deck slab of 16.5m effective width, which carries three-lane roadway. The height of girder is 2.2m and the maximum depth of the slab is 0.53 m. The deck of A-line is supported by means of 12 reinforced concrete twin columns, which nine of them are connected to an arch with a 265m span.

With regards to connection between girders and columns, the rigid structure is adopted on the tall columns and the crown. The isolated rubber bearings are used on the short

columns and abutments. The arch consists of a reinforced concrete 3cells-box-girder, 15.5m wide, with depth decreasing from 5.0m at the springing to 3.0 m at crown.

The arch is divided into two cantilevers with 27 segments. The length of each segment varies from 4.5 m to 5.5 m. The arch centerline describes a hyperbolic curve.

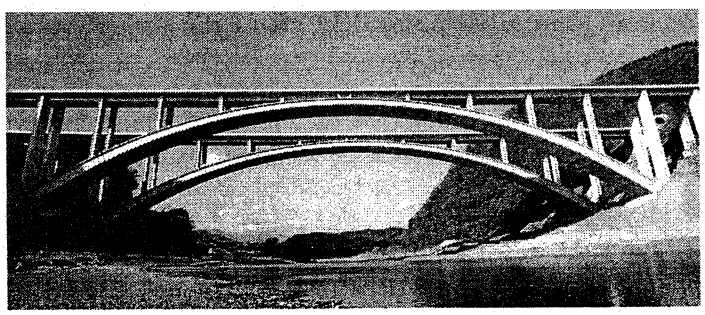

Photo 4: Fujikawa Bridge

4.3 Design
The bridges were designed with careful attention as follows.

(1) Assurance of resistance to major earthquakes
The bridges are not allowed being damaged seriously, even in case of major earthquakes, because they are a part of the most important expressway in Japan. Therefore, the seismic performance of the bridges is verified through controlling the following damages under large earthquakes,
1) Not to allow yielding of the steel girders and reinforcing bars in the slab
2) Only limited damages can be accepted for the arch and columns
Time history dynamic analyses were executed against major earthquake waves in order to calculate complicated response of the arch bridge under earthquakes, in consideration of material and deformation non-linearity. Bar modeling was applied in this analysis and all the members were modeled with fiber model to consider material non-linearity, variation of axial force and biaxial bending.

Moreover, careful attention was paid to increase ductility of the arch in structural details, including arranging of "intermediate stirrups" through the whole arch, and eliminating of lapping connection of re-bars where plastic hinges may be formed, and adopting rigid connection structure between the girders and the columns.

(2) Assurance of durability for long service life
For durability of concrete arch structure, concrete stress of the completed arch was designed to be compressive by using temporary stay cables during construction of cantilever arch. In addition, rust proofing for the steel girders was applied by blasting

melted high durable alloy of zinc and aluminum.

(3) Harmony between the bridges and the surrounding landscape
Aesthetic design was considered for harmony between the bridges and the surrounding landscape, such as emphasizing and shading edges of arch and columns, attaching walls to hide rubber bearings of girders for rhythm of columns, and selecting the girder's color like concrete for unification, etc.

4.4 Construction

The main erection phases are as follows,
Phase 1: Construction of substructures
Phase2: Cantilevering arch with temporary pylons, columns and stay cables
Phase3: Steel girders launching until the tips of the girders reach A1 abutment from A2 abutment
Phase4: Attaching prefabricated PC slabs from A2 abutment to A1 abutment.

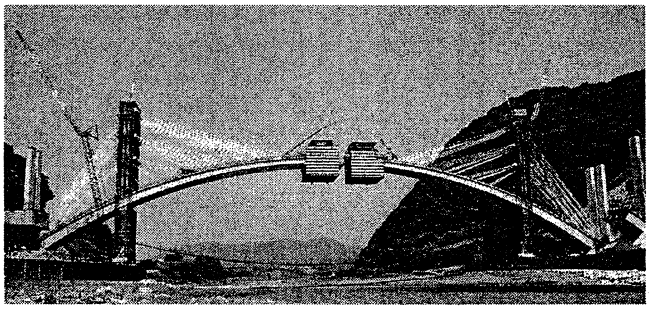

Photo 5: Construction of Cantilever Arch

5. Composite Truss Bridge

5.1 Sarutagawa Bridge and Tomoegawa Bridge

Sarutagawa Bridge and Tomoegawa Bridge, which adopt composite structures using steel-pipe on purpose to improve cost effectiveness, durability, seismicity and aesthetics. Sarutagawa Bridge and Tomoegawa Bridge, including in the scope of earthworks, have a total length of 1.2km. Each bridge consists of a three carriageway deck, 16.5m wide. Typical spans are 110m long for Sarutagawa Bridge and 119m long for Tomoegawa Bridge. The conjunction sections of these bridges, especially the most important panel sections that transmit shear force generated by axial force of trusses, have adopted two types of joint structures. One is double steel-pipe joint structure and the other is double friction gusset joint structure.

5.2 Design

Truss diagonals were made of light green-painted steel pipes. Fig.6 shows a general view

of the bridges. The most unique feature of these bridges is the fact that they are the world's first continuous rigid frame composite truss bridges, taking advantage of high earthquake-resistance making the best of high piers. The deck is 17.3m wide, carrying three carriageways. The deck structure is composed of two prestressed concrete slabs, which are held apart at the upper and lower levels by four inclined truss panels composed of steel diagonals, and connected directly to concrete slabs. The upper prestressed concrete slab is 0.27m thick, and is longitudinally stiffened by three ribs.

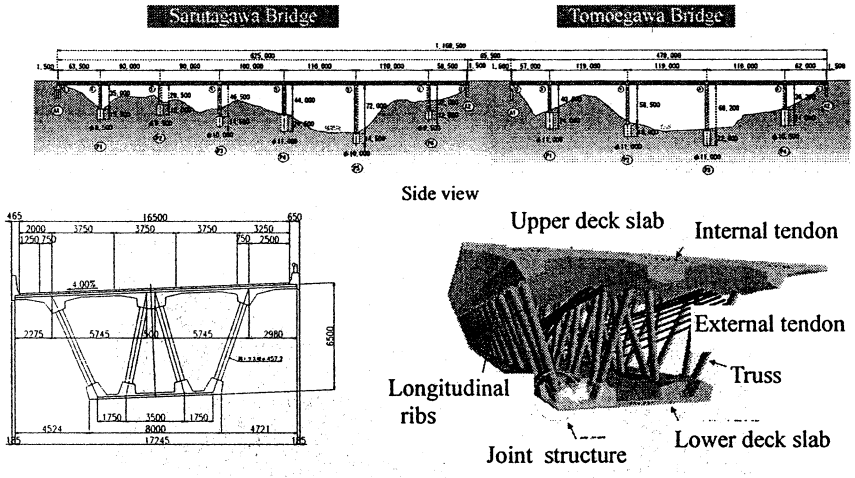

Figure 6: General view

The lower slab is variable from 0.25m to 1.04m thick and is ribbed in both directions to provide the necessary torsional rigidity to the deck. The deck is 6.50m height above the lowest part of the superstructure. Even if the girder is higher, there is almost no increase in the dead weight of bridge. Moreover, aesthetic design of pier and pier top segment are considered, because smooth transmission of force is symbolized by a reverse trapezoid combining a triangular texture, which seems to be a succession between the angles of trusses and a pier.

5.3 Joint Structure

The steel-concrete connection is one of the main characteristics of the structure. In the structure of a composite truss bridge, especially for the most important regions, which are connection sections between the concrete slabs and the truss diagonal, two types of joint structures have been adopted. One is a double steel-pipe joint structure shown in Fig.7 and the other is a double friction gusset joint structure shown in Fig.8. In order to apply cantilever erection method with form travelers to the bridges, the following functions are required to the joint structures.

(1) The joint structure should be not collapsed before other elements at the ultimate load.
(2) No cracking should be allowed of the concrete surrounding the joint structure at the design load.

Prior to its adoption, a static loading test with a 1/2 scale test specimen in shape of diagonal strutted was performed to verify the performance ensure safety and compatibility of detailed design.

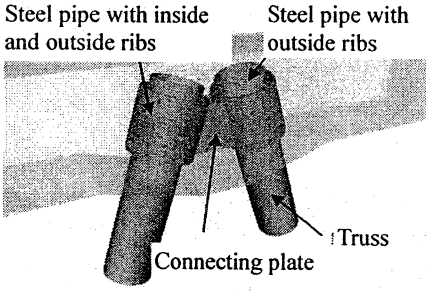

Figure 7: Double steel-pipe joint structure

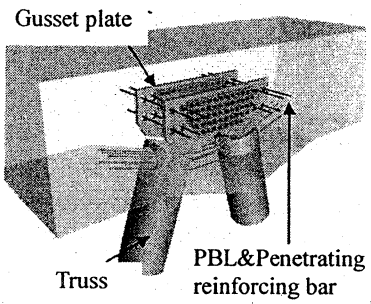

Figure 8: Double friction gusset joint structure

1. Double steel-pipe joint structure
The axial force of the truss is transmitted to the concrete by two outer pipes and a connecting plate. The trusses and outer pipes are separated by a concrete layer. The exterior ribbing of the truss pipes transfers the load through the concrete layer to the outer pipes, which are ribbed on both faces. The axial force is also transmitted through the truss as a shear force of the connecting plate and the SRC (Steel reinforced concrete) structure. This structure is economical, as designs can vary according to a level of axial force. This structure shows some characteristics as follows:

1) Economical designs are possible according to a level of axial force.
2) Quality control at the time of assembly is simple.

2. Double friction gusset joint structure
Due to the application of a friction grip connection of gusset plates connected to the trusses by fully penetrating reinforcing bars, shear force is transmitted through mostly steel materials. This structure shows some characteristics as follows:

1) It is possible to respond to high level axial force around pier top segment.
2) Because high strength bolts connecting with double friction gussets are adopted, the joints can be compact.

5.4 Conclusions
It is hoped that the experience of constructing these bridges will increase the applicable

span for PC composite truss bridges and lead to the adoption of two types of joint structures. It is believed that the adoption of PC composite truss bridges will increase in the future.

6. Conclusions

The technology of the PC Bridge in Japan has developed rapidly in the latest ten years. By adopting the hybrid structure, it increases the applicable span for the prestressed concrete bridge and it ensures structural endurance and retains economical efficiency. The hybrid bridges introduced in this paper have capability not only reducing the construction costs but also increasing the durability and reducing the maintenance costs.

7. References

1. Aoki K., Honma A., Yamaguchi T., and Hoshika M., "Design and construction of PC composite truss bridge," CONCRETE JOUNAL, Vol.42, No.8, pp.38-43, 2004.8
2. "National Report -Recent Works of Prestressed Concrete Structure-," Japan Prestressed Concrete Engineering Association, The Second fib Congress, 2006